

**NUMERICAL EVALUATION OF ENERGY LABELLING
TEST SETUPS OF CEILING FANS**

Dilshan Ramesh Casseer

188017V

Thesis submitted in partial fulfilment of the requirements for the degree of Master of
Science

Department of Mechanical Engineering

University of Moratuwa

Sri Lanka

October 2019

DECLARATION

I declare that this is my own work and this thesis does not incorporate without acknowledgement of any material previously submitted for a Degree or Diploma in any other University or institute of higher learning and to the best of my knowledge and believe it does not contain any previously published material or written by another person except where the acknowledgement is made in the text.

Also, I hereby grant to University of Moratuwa the non-exclusive right to reproduce and distribute my thesis/dissertation, in whole or in part in print, electronic or other medium. I retain the right to use this content in whole or part in future works (such as articles or books).

Name	Signature	Date
D.R. Casseer		

The above candidate has carried out research for the Masters thesis under my supervision.

Name	Signature	Date
Dr. R. A. C. P. Ranasinghe		

ACKNOWLEDGEMENT

This research would not have been a possible task without the immense support and assistance of many personnel. So, I would like to express my sincere gratitude to those who supported during the research.

Firstly, I would like to thank and appreciatively remind the research supervisors Dr. RACP Ranasinghe and Dr. P Kumarage, Senior Lecturers of Department of Mechanical Engineering, for their continuous guidance and supervision.

I gratefully acknowledge the University of Moratuwa senate research committee grant (Grant No. SRC/CAP/16/02), which supported this research.

I am greatly thankful to Mr. Wickrama, Director of Electrical and Electronic Division of Sri Lanka Standards Institution (SLSI) and the other staff members who supported in the ceiling fan testing facility for the experimental data gathering of the research.

I also acknowledge and extend my gratitude towards Technical Officer Mr. KT Priyantha and Lab Assistant Mr. Tharanga for the Aeronautical laboratory of university of Moratuwa for the related assistance throughout the period of this research.

Finally, I would like to express thanks to all my friends, academic, non-academic staff and other resourceful personnel who helped me in numerous aspects to accomplish this research successfully.

ABSTRACT

Ceiling fans are widely used as a means of providing thermal comfort to occupants in an indoor environment all around the world and it contributes to a significant portion of annual energy consumption throughout the world. A number of standards for efficiency analysis of ceiling fans are employed by many countries, with the intention of making ceiling fans more efficient. In these test standards, different test setups have been utilised. Work performed on analysis of the effect of these setups on performance evaluation of ceiling fans is currently unavailable. Further, there is a scarcity of research work performed on analysis of flow characteristics around a rotating ceiling fan. Understanding the proper flow around a rotating ceiling fan can lead to designing more efficient fan blades, which can lead to significant energy savings. Therefore, this study is split into two sections. In section one, a systematic investigation of the different test standards available for performance analysis of ceiling fans is performed, namely standards considered are ANSI/AMCA 230 standard, IEC 60879: 1986 standard, SLS 1600:2011 standard and Energy Star v1.2 standard for performance testing of ceiling fans. In section two, a flow physics analysis around a ceiling fan is carried out. For these, a CFD model was developed and it was validated using experimental results. The analysis of test standards was carried out by using a RANS method whereas the analysis of flow physics was carried out by using LES method. The numerical results obtained shows that the test cylinder present in some of the standards mentioned above, does not have a significant impact on the measured performance of the tested ceiling fan (variation is less than 2%), therefore having a test cylinder at an extra cost have no benefit on the measured results of ceiling fan testing. On the other hand, maintaining test cylinders for every fan size would impart a significant cost on the testing process and having a cylinder which is not correctly aligned can lead to inaccurate readings. From the flow results of the LES simulations, creation of two major vortical structures is seen arising from the tip and the root of the blade. As these vortical structures move further downward, more vortices were formed due to the action of these and the number of vortices keep growing with flow time, resulting the flow to become turbulent with the flow time. Furthermore, it was seen that the flow transition from laminar to turbulent occurred at the mid chord section, starting from the deflected section of the blade.

TABLE OF CONTENTS

Declaration	i
Acknowledgement	ii
Abstract	iii
Table of Contents	iv
List of Figures	vi
List of Tables	viii
1. Introduction.....	1
1.1 Aims	5
1.2 Objectives.....	5
2. Literature Review.....	6
3. Methodology.....	19
3.1 Experimental Analysis	19
3.1.1 Experimental Facility.....	19
3.1.2 Experimental Setup.....	19
3.1.3 Instrumentation	21
3.1.4 Test Procedures.....	23
3.1.5 Experimental Procedure.....	23
3.1.6 Derived Data Definition.....	24
3.2 Computational Modeling.....	28
3.2.1 Model of the Fan.....	28
3.2.2 Mesh Generation.....	31
3.2.3 Turbulence Modeling.....	33
3.2.4 Solver Setup.....	34
3.2.5 Simulation of Motion of Blades.....	35

3.2.6	Boundary Conditions	37
3.2.7	Cell zone conditions.....	38
3.2.8	Initialization and Calculation.....	38
3.2.9	Analysis of the Effect of Ceiling Fan Test Chamber Geometry on the Performance Measurement of Ceiling Fans	39
4.	Results.....	41
4.1	Experimental Results.....	41
4.1.1	Assumptions.....	41
4.1.2	Results.....	41
4.2	CFD Simulations.....	43
4.2.1	Case 1: Analysis of The Effect of Ceiling Fan Test Chamber Geometry on The Performance Measurement of Ceiling Fans.....	43
4.2.2	Case 2: Analysis of The Flow Field Characteristics Around Rotating Ceiling Fan Blades	52
5.	Discussion.....	56
5.1	Experimental Data.....	56
5.2	Case 1: Analysis of the effect of ceiling fan test chamber geometry on the performance measurement of ceiling fans	59
5.3	Case 2: Analysis of the Flow Field Characteristics Around Ceiling Fan Blades.....	65
6.	Conclusion	75
7.	References.....	77

LIST OF FIGURES

Figure 1.1 – Flow profile generated by a ceiling fan.....	2
Figure 2.1 - Variation of flow coefficient with ceiling height	9
Figure 2.2 - Standard test chamber setup as per SLS 1600:2011 standard.....	10
Figure 2.3 - Energy star v1.2 standard for ceiling fan testing.....	11
Figure 2.4– IEC 60879 standard	11
Figure 2.5 – Von Karman Vortices at the trailing edge of a propeller blade	16
Figure 2.6 – Tip vortices illustration using iso surfaces of Q-Criterion	17
Figure 2.7 – Vortex identification using Q criterion	18
Figure 3.1 - Standard test chamber setup.....	19
Figure 3.2 – Test chamber containing the cylinder and the placement of anemometer sensors...	20
Figure 3.3 - Anemometers probe and DAQ card.....	22
Figure 3.4 – Digital Power Meter	22
Figure 3.5 – Placement of the Anemometers.....	24
Figure 3.6 – 3D Model of the ceiling Fan.....	29
Figure 3.7 – Fan rotor dimensions	30
Figure 3.8 – CFD domain	30
Figure 3.9 – Close view of moving section	31
Figure 3.10 – Mesh in the moving region.....	32
Figure 3.11 - Cross Sectional view of the mesh	32
Figure 4.1 – Spatially and time averaged experimental data	42
Figure 4.2 – Measured parameters at different regulator settings	43
Figure 4.3 – Variation of output parameters with mesh size	44
Figure 4.4 – Effect of the turbulence model on the output velocity for turbulence models	45
Figure 4.5 – Comparision of axial velocity results of SA model with experimental results	46
Figure 4.6 – Simulated Results	47
Figure 4.7 – Generated velocity distributions.....	48
Figure 4.8 - Effect of the gap between the plane of rotation of the fan and the test cylinder.....	49
Figure 4.9- Effect of height of the test cylinder.....	50
Figure 4.10- Effect of diameter of the test cylinder.....	51
Figure 4.11 - Effect of the size of the test chamber	52

Figure 4.12 – Axial velocity variation	53
Figure 4.13 – Output value variation with mesh size	54
Figure 4.14 – Computational results for the selected RPM	55
Figure 4.15 – Area averaged results of 7 points at 0.1m intervals in radial direction just below the cylinder	55
Figure 5.1 – Measured parameters at different regulator settings	57
Figure 5.2 – Comparison of axial velocities 1m below the plane of rotation of fan	59
Figure 5.3 – Comparison of axial velocities at a height of 1m below the plane of rotation of the fan between a case with and without a test cylinder	60
Figure 5.4 – Comparison of calculated values between tested cases.....	62
Figure 5.5 – Comparison of calculated values between cases of different room sizes.....	64
Figure 5.6 – Spatially averaged axial velocity variation of 120^0 angle along radii of the ceiling fan with time	65
Figure 5.7 – Variation of axial velocity at 8 points at 100mm intervals along the radii of the ceiling fan with time in 5 lines along the radii of the fan at 30^0 intervals	66
Figure 5.8 – Instantaneous velocity vectors at 8 equally spaced points on one line at different flow times in comparison with experimental data.	67
Figure 5.9 – Formation of vorticial structures	68
Figure 5.10 – Vertical contour of velocity through centre of rotation of fan	69
Figure 5.11 – Iso surface of $Q=3000 \text{ s}^{-2}$ colored by velocity magnitude.....	70
Figure 5.12 – Iso surface of vortex core region at Vorticity = 250 s^{-1} colored by velocity.....	71
Figure 5.13 – Formation of vorticial structures	72
Figure 5.14 – Instantaneous contours of vorticity at vertical planes of $x=12\text{mm}$, 24mm and 36mm at a flow time of 3.299s	72
Figure 5.15 – Vorticity contour on the bottom surface of the blade.....	73
Figure 5.16 – Total pressure in the mid -chord section of the fan blade	74

LIST OF TABLES

Table 2.1 – Comparison of major dimensions of ceiling fan test standards	12
Table 3.1- Parameters evaluated during simulations	40
Table 4.1 – Measured RPM values	41
Table 4.2 – Flow parameters at different RPMs	42
Table 4.3- Variation of output with mesh size.....	44
Table 4.4 -Calculated RMSD between cases using different turbulence models	45
Table 4.5- Calculated NRMSD between simulated case using SA turbulence model and experimentally measured values for the five test cases	46
Table 4.6- Variation of output with mesh size.....	53
Table 5.1 – Flow parameters at different RPMs	56
Table 5.2 – Key for energy rating as per SLS 1600:2011	58
Table 5.3 – NRMSD w.r.t. a case without test cylinder	61
Table 5.4 – Summary of calculated service value and flow coefficient in cases with different cylinder geometries.....	63
Table 5.5 – Calculated energy rating of different cases.....	63

1. INTRODUCTION

Ceiling fans are widely used as a common household and office appliance in both old and new buildings all around the world and these are very popular in tropical regions in Asia, USA and Europe. Although the use of air conditioners for maintaining thermal comfort in commercial buildings and households is becoming popular, it is shown that using a ceiling fan in an air-conditioned environment can lead to higher thermal comfort levels at a higher efficiency than using an air conditioner alone [1]. Ceiling fans produce non-uniform velocity profiles, resulting in non-uniform thermal environments, which in turn lead to more thermally comfortable environments [2]. In previous research, it is shown that having an air velocity of 1ms^{-1} can induce same thermal comfort level as lowering the temperature by 4.5°C , up to a room temperature of 29°C [3]. Therefore, making ceiling fans more energy efficient is an important area of research which can potentially lead to considerable energy savings in many countries.

Ceiling fans contribute significantly to annual global energy consumption. It is shown that comfort fans accounts for 3 to 4 TWh of electricity consumption each year in Europe [4]. In India, 6% of total residential energy consumption in 2000 is accounted for ceiling fans, and this is expected to grow to 9% by 2020 [5]. Further, 5.7% of energy consumption by commercial buildings in western state of Gujarat in India is accounted for ceiling fans. 79% of urban households of Sri Lanka is said to have at least one fan and 50% of these are ceiling fans. This accounts to 126GWh of electrical energy use per year in Sri Lanka as at year 2000 [6]. Therefore, making ceiling fans more energy efficient is an important consideration which can potentially lead to considerable energy savings. In the recent past, many studies have been performed on ceiling fans and various standards have been brought forward in different countries. In US, EnergyStar certification has been introduced for ceiling fans and EnergyStar certified fans are said to be 40% more efficient than conventional fans [7]. In Sri Lanka, Star rating have been introduced based on the efficiency of the ceiling fans [8]. In India, schedule 8 has been brought forward for energy efficiency labelling for ceiling fans [9].

The flow field in ceiling fan is affected by the vortices formed on the rotating blades of the fan. Mainly, the vortices identified are tip vortices, root vortices and hub vortices [10]. Further, the

surrounding physical environment, namely the distance from the rotor to the ceiling and the surrounding walls characterise the flow generated by a ceiling fan [11]. Also, the operational and design characteristics such as the number of blades, solidity of the rotor and the speed of rotation of the fan governs the flow field [10].

The flow jet produced by a ceiling fan expands as it moves downwards, due to the transfer of momentum to surrounding particles. Further, the jet flows in reverse direction along the walls of the room, towards the suction side of the fan, in turn creating a circulating flow. A buffer layer is present between this reverse flow and downward flow, originating from the tip of the fan blade [11]. This is illustrated in the diagram below.

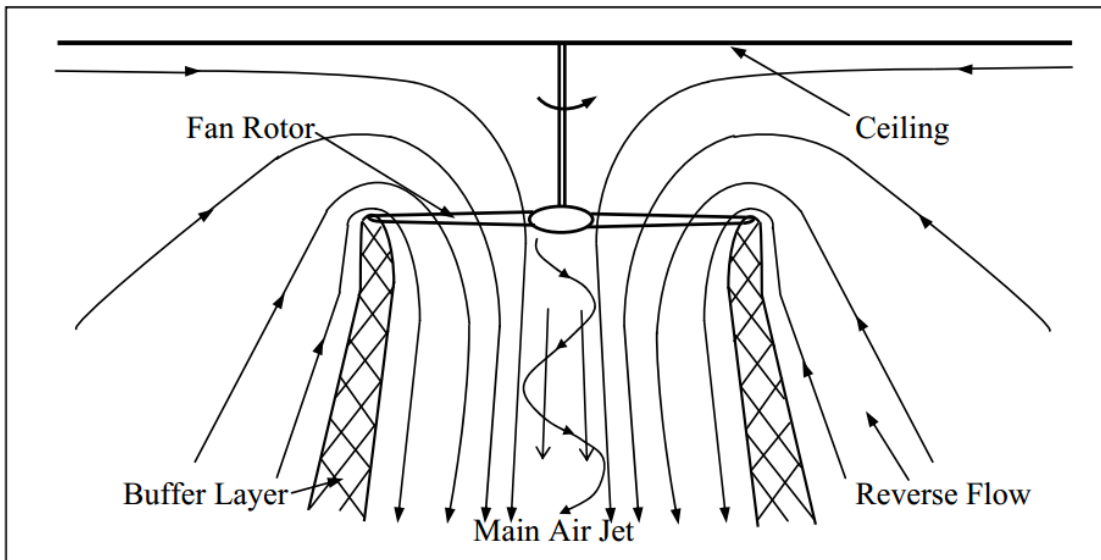


Figure 1.1 – Flow profile generated by a ceiling fan [11].

The major potential ceiling fan efficiency improvement aspects with most effect on the efficiency are the motor and the blades [12]. In ceiling fans, mechanical energy is produced by transforming electrical energy by the rotation of a motor shaft through a speed controller. Kinetic energy is then produced by interaction with the blades with surrounding air resulting in an airflow. Energy losses are prevalent on each of these conversion steps, collectively contributing to total efficiency of a ceiling fan. But it is shown that the major portion of the losses occurs at the blades, due to their aerodynamic characteristics [13]. Though there are ceiling fans with numerous blade designs, thin bladed fans are used most popularly in the commercial and household market [14] [15]. Therefore, the scope of this research is limited to analysing the aerodynamic performance and flow delivery of ceiling fans with thin blade profiles under different operating conditions.

For the quantitative analysis of the efficiency of ceiling fans and to obtain the star rating for ceiling fans, a number of standards have been brought forward by many institutions, [7] [16] [8] such as the IEC 60879: 1986 introduced by International Electrotechnical Commission [17], ANSI/AMCA 230 introduced by Department of Energy USA [18], IS:374-1979 supplemented by Schedule 8 brought forward by Bureau of Energy Efficiency and Bureau of Indian Standards [9] [19] and SLS Standard 1600:2011 introduced by Sri Lanka Standards Institution (SLSI). In these standards, a test setup which is to be utilised in the velocity measurement, and efficiency calculation of ceiling fans has been introduced. The standards which are aimed at the energy rating evaluation of ceiling fans such as ANSI/AMCA 230, SLSI 1600:2011 and Energy Star v1.2 have employed a test cylinder which is placed below the fan in order to direct the diverging flow field generated by the ceiling fan towards the anemometer sensors, avoiding the buffer layer.

The placement of this test cylinder and its geometry is defined arbitrarily in these standards and is different from one standard to another. Clear background research on selecting the geometry parameters of these setups such as the gap between the fan and test cylinder, size and height of the test cylinder is not available. I.e.- In Sri Lanka Standard 1600:2011, a cylinder of same diameter of the fan is required to be suspended 75mm below the plane of rotation of the fan [8] where as in the method forwarded by Energy Star USA, a cylinder of diameter 200mm more than that of the fan under test is required to be placed 152mm below the plane of rotation of the ceiling fan [20]. Further the International Electrotechnical Commission (IEC) 60879 standard, which is the basis of national standards of many countries such as India, Pakistan, Bangladesh, China, Vietnam, Indonesia, does not contain a cylinder in the test setup, however this contains a box with an opening level with the plane of rotation of the fan, allowing the airflow from the fan to reach the anemometer sensors inside the said box [9] [21]. The test chamber size in each standard is also different from one another, it is given as 3600x3600x3000 in SLS 1600:2011 standard whereas it is specified as 6096x6096x3352 in US standard and 5500x5500x3000 in IEC standard, all dimensions given as WxLxH (mm) [17] [9] [18] [8].

Through a thorough literature review, scarcity of research on in depth analyses of the flow field produced by a ceiling fan was identified. A proper understanding on how the ceiling fan blades interact with the air flow could lead to implement fan blade designs that would increase the

aerodynamic efficiency of ceiling fans. Computational Fluid Dynamics (CFD) is a tool which can be used suitably for this analysis.

Thereby, this research is divided into two sections to analyse standard ceiling fan test conditions and flow field characteristics around a rotating ceiling fan, as given below.

1. Analysis of the effect of ceiling fan test chamber geometry on the performance measurement of ceiling fans.
2. Analysis of the flow field characteristics around a rotating ceiling fan blades.

Both the analyses are performed by developing CFD models. The software used for this purpose is commercial CFD code, ANSYS Fluent. For the validation of the CFD cases, the flow field obtained was compared with experimental data obtained at the experimental setup of the same case at the fan testing laboratory at the Sri Lanka Standards Institution (SLSI).

The practical flow in a ceiling fan is unsteady in nature as a result of inlet distortion, vortices, secondary flows, and turbulence [22]. Therefore, in order to obtain a more accurate numerical solution, the numerical modelling should be done at unsteady state. In the recent past, the computational power of accessible resources has increased drastically. This enables accurate prediction of an unsteady flow more conceivable for the researches. There is a lack of researches done on ceiling fans by using CFD models. And out of those, only a few are prevalent simulating unsteady flow.

Therefore, in this research, a three-dimensional transient case has been set up for accurate analysis of the flow field characteristics, including vortex formations. Sliding mesh method was incorporated in this study to simulate motion since it can accurately solve for unsteady cases [23]. For the analysis of the effect of test chamber geometry on the flow field of the ceiling fan, steady state calculations were used with MRF method, as they are computationally less expensive. As turbulence modeling, Large Eddy Simulation was used for flow field analysis in order to obtain more accurate results and to visualise eddy formulations while RANS methods were used for analysis of the effect of the test chamber geometry on the generated flow field, due to the computational advantage those offer.

The effect of the ceiling fan test chamber geometry parameters on the efficiency measurement of ceiling fans and the flow field characteristics around a rotating ceiling fan was identified using the obtained results. Using this data, possible changes to the efficiency measurement standards of ceiling fans that can lead to potential increase in accuracy of performance analysis and cost savings were identified. The identified flow characteristics around the rotating ceiling fan can be used in further research to develop a more efficient thin bladed fan design, that can lead to considerable amount of potential energy savings.

1.1 Aims

1. To analyse the flow field around ceiling fans with thin blade profiles in standard test conditions
2. To investigate the effect of standard ceiling fan test setup geometry on the same via numerical methods.

1.2 Objectives

1. To develop a methodology for analysing the aerodynamic characteristics around a ceiling fan in operation.
2. To analyse the effect of prevailing standard ceiling fan test setup on the measured performance of the ceiling fans.
3. To suggest potential changes to the standard ceiling fan test setup to facilitate more accurate measurements of efficiency of ceiling fans.

2. LITERATURE REVIEW

Ceiling fans are used popularly in tropical countries in order to maintain thermal comfort at a considerably low cost. It is important to assess the efficiency of the ceiling fans due to the extensive number of ceiling fans in use by the general public. It is seen that in India, 6% of total residential energy consumption in 2000 is accounted for ceiling fans, and this is expected to grow to 9% by 2020 [5]. Further, it has been pointed out that comfort fans accounts for 3 to 4 TWh of electricity consumption each year in Europe [4].

In another research published by Ernest Orlando Lawrence Berkeley National Laboratory, USA has pointed out that ceiling fans are mainly designed focusing on aesthetic aspect and ease of fabrication rather than focusing on the aerodynamic efficiency of the fan [24]. Further it states that “ceiling fan efficiency can be cost-effectively improved by at least 50% and if these improvements are implemented in all ceiling fans sold by 2020, 70 terawatt hours per year & 25 million metric tons of CO₂ could be avoided” [12].

It is further seen that 79% of houses in urban Sri Lanka is stated to have at least 1 fan for thermal comfort and out of this, 50% is said to be ceiling fans. This amounts to a significant portion of national energy consumption per year in Sri Lanka, amounting to 126GWh as at year 2000. In this research, it is further highlighted that an energy saving of 31GWh per year can be achieved by utilising more efficient ceiling fans [25].

United States Energy Information Administration (EIA) estimates that the largest consumption of energy in USA in the year 2017 is for space cooling which amounts to 15.4% of total national energy use [26].

Further, According to a survey study conducted in China by Tsinghua University, it is seen that 70% of survey participants have reported that they use fans at home, even if air-conditioning is available [27].

In this regard, the importance of maintaining standards of commercially made ceiling fans is shown. In India, Super-Efficient Equipment and Appliance deployment (SEAD) program and Super-Efficient Equipment Program (SEEP) have identified the necessity of maintaining the efficiency of commercially made ceiling fans [12]. In USA, an energy star labelling has been introduced by Environmental Protection Agency (EPA), with the intention of increasing the

efficiency of commercially available electrical appliances, including ceiling fans. These energy star certified ceiling fans are said to be 40% more efficient than non-energy star certified ceiling fans [28]. In Sri Lanka, Star rating has been introduced based on the efficiency of the ceiling fans [8].

In the article “Energy Efficiency Policies in India: Implications for Climate Change Mitigation” it is highlighted ceiling fans as one of the key appliances that can lead to a significant potential energy saving by the introduction of a Standards and Labeling program in India, and this potential saving is calculated as 136.8 Billion Units by 2030 [29].

Considering these facts, it is evident that efficiency of ceiling fans should be of consideration and making ceiling fans more efficient can lead to a significant change in the worldwide energy consumption, for the better. Thereby, standards institutions of many countries have brought forward numerous test standards to regulate efficiency measurement and minimum energy performance of ceiling fans.

The IEC 60879: 1986 has been introduced by International Electrotechnical Commission [17], ANSI/AMCA 230 has been introduced by Department of energy USA [18], CSA-C814-10 has been brought forward by Canadian Standards Association [30], IS:374-1979 supplemented by Schedule 8 brought forward by Bureau of Energy Efficiency and Bureau of Indian Standards [31] [19], for this purpose.

In Sri Lanka, Sri Lanka Standards Institution has introduced an energy star label for ceiling fans with the intention of increasing the overall efficiency of the same [8]. This would allow customers to identify more efficient fans.

The efficiency of ceiling fans is mainly dependent on the motor and the blades [12]. Ceiling fans produce air flow by using the mechanical energy produced by an electrical motor which converts electrical energy to kinetic energy by the action of rotating a shaft via a speed controller. This Kinetic energy is used by the blades to produce airflow by interaction of the blades with the surrounding air. Though energy losses are prevalent on all of the energy conversion steps, it has been shown in previous work, that majority of losses occur at the blades, due to aerodynamic characteristics [13].

The flow field around a rotating ceiling fan and its creation are discussed in the work “Wall Effects

on The Performance of Ceiling Fans: A Two-Dimensional Model” [11]. In this, it is stated that jets of air are discharged due to pressure jump created across the fan rotor as a result of rotation of the fan blades. The fan draws air from converging reverse flow stream, which is located outside of the downward air jets. This downward air stream diverges as it moves further away from the fan, since adjacent layers of air is also accelerated downwards due to the action of shear forces. A buffer region is also present between the downwards and reverse flow, which is of large scale turbulence. This is illustrated in figure 1.1.

This flow region is further investigated in the research “Experimental Investigation of the Flow Field of a Ceiling Fan” [24]. In this work, it is stated that the highest velocities inside a typical room ventilated by a ceiling fan are present directly below the fan. These velocities are in the order of $2-3 \text{ ms}^{-1}$. This flow region is turbulent, three dimensional and periodic in nature and consists of a substantial amount of swirl. The downward air flow is determined to be diverging in a conical shape, at an angle of 10° . The diameter of the cone, just below the fan is said to be 10-15% lower than the diameter of the fan blades. The flow velocity of the reverse flow is less than 0.1 ms^{-1} in the lower region, after which it accelerates and gains both radial and vertical velocity.

In another previous work, it is elaborated that the flow jet produced by a ceiling fan expands as it moves downwards, due to the transfer of momentum to surrounding particles [32]. Further, the jet flows in reverse direction along the walls of the room, towards the suction side of the fan, in turn creating a circulating flow. A buffer layer is present between this reverse flow and downward flow, originating from the tip of the fan blade.

The flow field creation in ceiling fan is affected by the vortices formed on the rotating blades of the fan. Mainly, the vortices identified are tip vortices, root vortices and hub vortices [10]. The most dominant vortices are formed at the tip of the fan blades. These vortices hinder the downward flow in the vicinity of the blade tip. Therefore, due to the action of this vortex, only about 75% of the blade is utilised for the generation of the downward flow [24]. This in turn affects the efficiency of the ceiling fan.

The physical geometry around the operating ceiling fan, such as the distance from the rotor to the ceiling and distance from the fan to surrounding walls also affect the flow field produced by it [11]. Further, this flow field generated by ceiling fans is also affected by the design characteristics

such as number of blades of the fan, solidity of the blades and operational characteristics such as speed of rotation of the fan [10].

The generated airflow is decreased when the distance from the ceiling to the fan rotor is decreased. It has been shown that the flow increases rapidly from zero until the ratio, ceiling height (H)/ Fan radius (R) is close to one. The flow generated at 1 H/R is around 85% of flow generated without a ceiling [11]. This is illustrated by the figure 2.1 below.

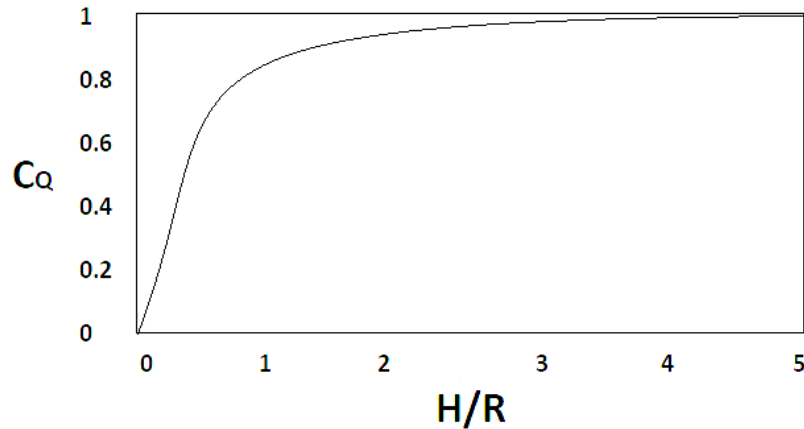


Figure 2.1 - Variation of flow coefficient with ceiling height [11]

Flow Rate of ceiling fans is increased with the number of blades and the flow becomes more uniform. However, the overall efficiency of the ceiling fan is decreased when the number of blades is increased [33].

In the research work “Measured Ceiling Fan Performance and Usage Patterns: Implications for Efficiency and Comfort Improvement” [34], it is stated that the increase in flow rate and power consumption of fans is decreasing with the RPM. i.e. though the power consumption and flow rate are increasing with RPM, the ratio of the two with the previous RPM will be decreasing. This further states that the cfm/W value will also decrease when the speed of rotor is decreased.

The efficiency measuring procedures for the ceiling fans forwarded in the SLS 1600:2011 standard, is as follows. The Testing chamber should be a completely enclosed room of dimensions 3600mm in length, 3600mm in width and 3000m in height. The test chamber should also contain a cylinder of diameter as same as that of the fan and 600mm of height, placed 75mm below the plane of rotation of the fan [8].

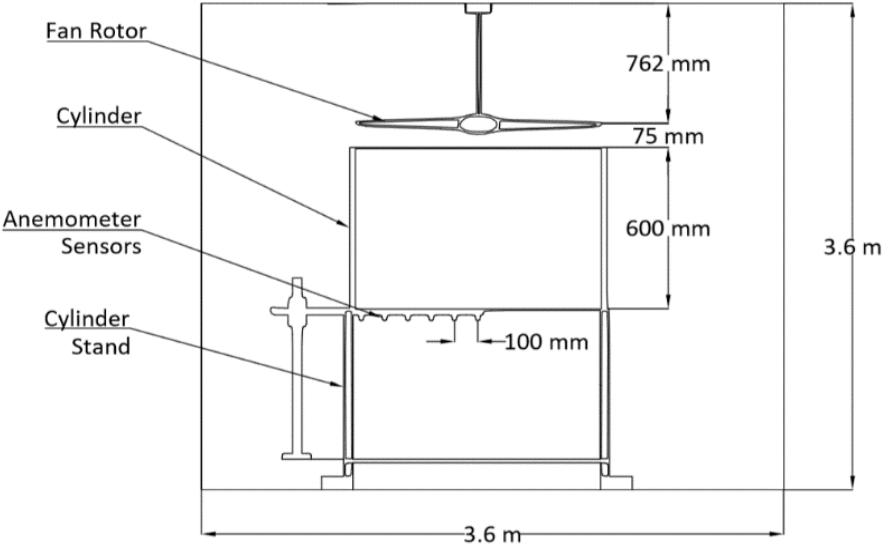


Figure 2.2 - Standard test chamber setup as per SLS 1600:2011 standard

In energy star standard for ceiling fan testing v1.2 of USA, a cylinder of diameter 200 mm more than that of the fan under test and height 914 mm is required to be placed 152mm below the plane of rotation of the ceiling fan, in a room of 3352 mm height, 6096 mm width and 6096 mm length. This room should also be free from any external disturbances [20].

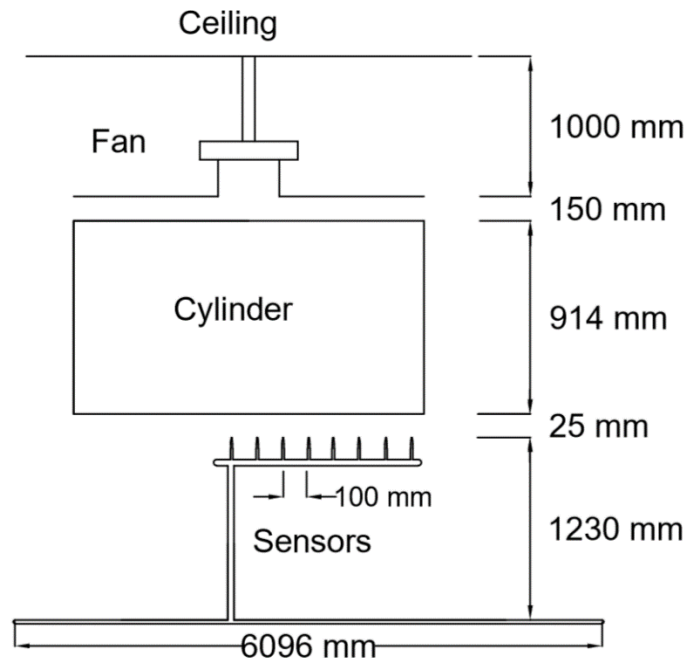


Figure 2.3 - Energy star v1.2 standard for ceiling fan testing

The International Electrotechnical Commission (IEC) 60879 standard is used as the basis of national standards of many countries such as India, Pakistan, Bangladesh, China, Vietnam and Indonesia. In this standard, a box of size 4500 mm length and 4500 mm height and 3000 mm height is required to be present in a room of size 5500mm length and 5500mm width. A cut as the same diameter as the fan should be present in this box, and the fan should be suspended in the centre of this cutout, level with the box. Anemometer sensors are placed inside this box.

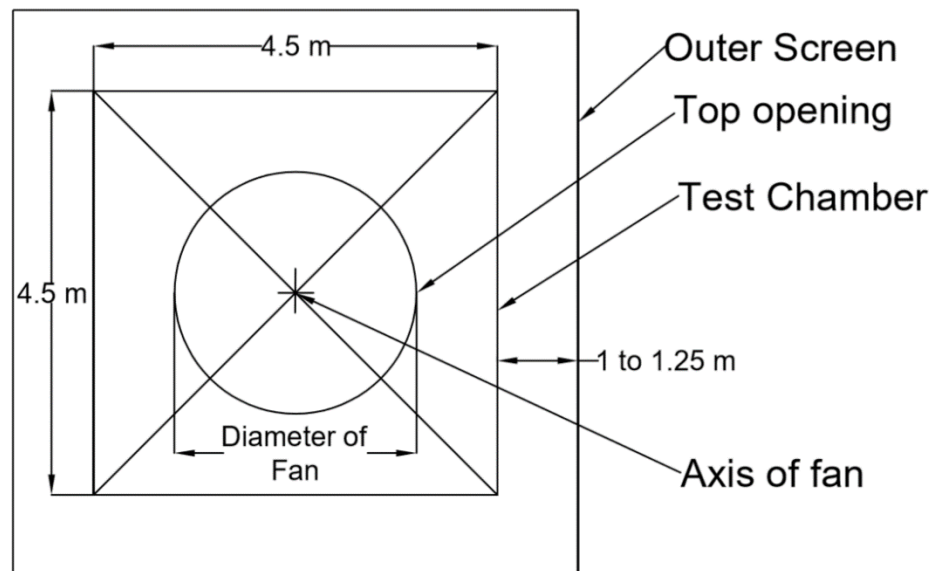


Figure 2.4– IEC 60879 standard

The CSA-C814-10 standard of Canada is based on US standard and has no appreciable difference between them [35].

The differences between these standards is summarised in the table below.

Parameter	ANSI/AMCA 230	IEC 60879: 1986	Energy Star v1.2	SLS 1600:2011
Room Size (mm x mm)	6096 x 6096	5500 x 5500	6096 x 6096	3600 x 3600
Room Height (mm)	3352	3000	3352	3000
Diameter of Test Cylinder (mm)	No cylinder used	Instead of a cylinder, a Chamber of 4500 x 4500 used	200 larger than the fan diameter	Same as test fan diameter
Height of Test Cylinder (mm)	No cylinder used	No cylinder used	914	600
Gap Between Fan and Cylinder (mm)	No cylinder used	No cylinder used	150	75
Gap Between Fan and Ceiling (mm)	1000	1000	1000	762
Location of Air Velocity Sensors (mm)	1100 below the fan	1500 below the fan	25 below the cylinder (1100 below the cylinder)	Just below the test cylinder (675 below the fan)

Table 2.1 – Comparison of major dimensions of ceiling fan test standards

As shown above, in many ceiling fan efficiency measurement standards such as ANSI/AMCA 230, CSA-C814-10, SLSI 1600:2011 have employed a test cylinder which is placed below the fan in order to direct the diverging flow field generated by the ceiling fan towards the anemometer sensors, avoiding the buffer layer [18] [30] [8].

The standard test geometry is different from one standard to another, as seen from the above comparison. Further, the relationship between parameters such as gap between cylinder and plane of rotation of fan, cylinder height, cylinder size and the efficiency measurement are not established.

Clear research on how these parameters have been defined in the test standards is also not available.

In order to evaluate the generation of flow fields and calculate different parameters, analytical modeling, numerical modeling and experimental analysis are being used extensively [36]. Experimental analysis is time consuming and significant cost and effort needs to be expended to obtain accurate measurements.

Therefore, for this purpose, Computational Fluid Dynamics (CFD) is used popularly both in research and in the industrial applications. These programs work on laws of conservation of energy, conservation of mass and conservation of momentum [23]. Popular CFD software's in use are ANSYS Fluent, Open Foam, Flow 3D, Star CCM. Out of these ANSYS fluent is the most popularly used package, due to its ease of use, greater support and development and since it contains a comprehensive package [37].

CFD software packages mainly employ Navier Stokes equation in prediction of complex fluid flow. This equation is solved numerically, in combination of any other relationship present according to the flow problem in CFD software, since a known analytical solution is not present for that equation [38].

Turbulence is a three-dimensional and time-dependent phenomenon occurring in fluid flows due to the viscous effects. Turbulent flows are complex and modeling of these flows is less precise due to this complex nature. In CFD, in order to model the effect of turbulence, mainly three methods are used. These are Direct Numerical Simulations (DNS), Large Eddy Simulations (LES), and Reynolds-Averaged Navier-Stokes (RANS) simulations. DNS is very accurate in modeling turbulence but is computationally very expensive. On the other hand, RANS do not require much computational power when compared with DNS. One RANS model is not applicable for all fluid problems, and the accuracy of the results are acceptable, but is on the lower side. LES use both DNS and modeling approaches and is computationally advantageous to be used. It provides far better results than RANS techniques, therefore though it is computationally expensive than RANS, it is being used more popularly due to its accuracy and ability to predict the formation of eddy flows [39].

The acceptable simulation time for a transient simulation is given as $t = 6.28 1/\pi n$, where t is the time in seconds and n is the speed of rotation in RadS^{-1} . The appropriate time step for this purpose can be taken as $\Delta t = 1.936 \times 10^{-5} (1/\pi n)$ [40].

The practical flow in a ceiling fan is unsteady in nature as a result of inlet distortion, vortices, secondary flows, and turbulence [22]. Sliding mesh method can be used simulate motion in unsteady cases with a higher accuracy [23].

In the work “Investigating Aerodynamic Performance of a Ceiling Fan” MRF method has been used successfully along with RANS simulations for a steady simulation for a rotating ceiling fan. The results are shown to be in good agreement with the experimental results [41].

Fluent User Guide describes central differencing scheme as an idea choice for spatial discretization for LES, but can often lead to unphysical oscillations. Therefore, Bounded Central Differencing scheme is recommended for spatial discretization for LES [23].

Ansys guide for LES simulations states that in order to run LES simulations, the simulation should be performed by RANS model initially. And this should be run done by using 2-equation RANS models. RNG KE and SST KW is recommended for this purpose. Once the flow has been developed, it is recommended to switch to LES [42].

For steady state calculations of a ceiling fan using RANS method, it is shown in previous research standard K-Epsilon (KE), standard K-Omega (KW) and Spalart Allmaras (SA) model has been evaluated and it is indicated that Spalart Allmaras model gives the results closest to experimental results [41].

SA model is a one-equation transport model used for turbulence modeling RANS simulations. This model is compatible of any grid structure and it is shown that this model yields acceptable results for indoor simulations [43]. Further, it is shown in previous research that this model yields results closer to experimental results for a similar case [41].

The KE model is a two-equation transport model used for turbulence modeling in RANS simulations. These two equation models are expected to give superior results than one equation models, but the results would depend on the specific case. The KE model is widely used for indoor airflow simulations [44]. Though the standard KE model is mainly applicable to high Reynolds

number (Re) flows it can be applied for low Re flows with wall functions to model flows in the vicinity of walls [45].

The RNG KE model has also been widely used for indoor flow simulations [46]. It has been validated for air distributions in an office space and a classroom and it is shown that the results are in good agreement with experimental results [47].

The KW model is another two-equation transport model. This is known to give improved results than KE model in adverse pressure flows. This model has also been used for indoor air distribution simulations and is known to give good results [43].

In LES, The Wall-Adapting Eddy-Viscosity (WALE) model is used to model subgrid scale viscosities and is designed to return the correct wall asymptotic behavior for wall bounded flows [48]. It has a simplicity closer to Smagorinsky-model, which is the simplest subgrid model but has a higher accuracy in predicting near wall behavior of flow. Therefore, WALE model can yield better results with good accuracy in large eddy simulations, with a considerable simplicity in calculations [49].

Further, results obtained by using WALE model for a case of a turbine simulation using LES is said to be in good agreement with experimental results, compared to Smagorinsky (SM), Dynamic (DM) and Scale-Dependent Dynamic (SDDM) subgrid models [50].

In the work “Large-Eddy Simulation of the Flow Field in a Rotating Axial Fan” the flow contours of a rotating axial fan are illustrated. It states that a small counter-rotating separation vortex appears near the leading edge of the rotating blade which has very low turbulent kinetic energy [40].

A comparison of experimental data with data gathered from LES of an Axial Compressor Rotor has shown that LES reproduces main qualities of the flow and are in good agreement with experimental results. [51]

In the research work titled “Cut-cell method based large-eddy simulation of tip-leakage flow”, the tip leakage vortex resulting due to the pressure difference between suction and pressure side of a axial rotor is visualised using LES method [52].

In the article “On the onset of wake meandering for an axial flow turbine in a turbulent open channel flow”, it is shown that the simulated results from LES simulation of an axial flow turbine

are in good agreement with the experimental measurements. It further states that an axial turbine consists of two wakes consisting of a tip vortex shear layer rotating in the direction of the turbine rotor and a counter rotating hub vortex. These tip vortices have been identified by the use of iso surfaces of velocity magnitude [53].

In order to present the vortices produced by a fixed wing aircraft in motion, contours of vorticity magnitude generated by LES simulations in different planes of 40m apart at different time intervals have been utilised. To further illustrate these vortices, iso surfaces of vorticity magnitude have been employed. This method accurately illustrates the vortices formed in the wake of the aircraft [54].

It is illustrated in the paper “Study on Practical CFD for Unsteady Vortices from Trailing Edge of Propeller Blades” that Von Karman vortices are produced at the trailing edge of the propeller blade of a marine vessel in alternating regular patterns in two separate rows. This illustration has been done by RANS and LES models [55].

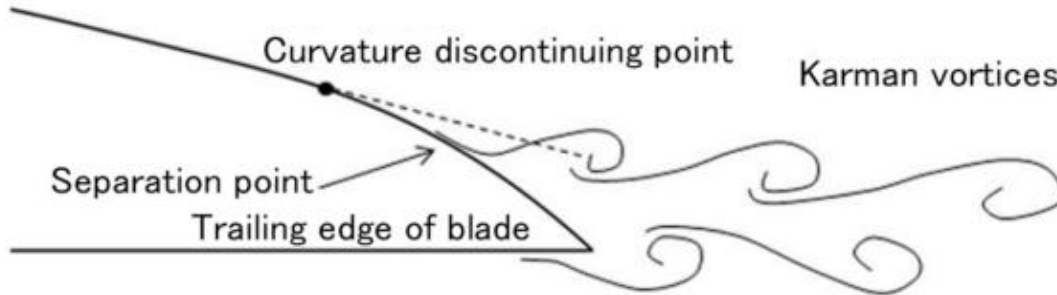


Figure 2.5 – Von Karman Vortices at the trailing edge of a propeller blade [55]

Q criterion is used popularly for vortex identification in fluid dynamics [56]. Q criterion is defined as the balance between rotation rate (Ω_{ij}) and strain rate (S_{ij}). Therefore, Q criterion can be used to identify the areas where the strength of rotation overcomes the strain, which in turn means that the same area is rotating, indicating a vortex [57].

$$\Omega_{ij} = \frac{1}{2}(u_{i,j} - u_{j,i}) \quad (1)$$

$$S_{ij} = \frac{1}{2}(u_{i,j} + u_{j,i}) \quad (2)$$

$$Q = \frac{1}{2}(\Omega_{ij}^2 - S_{ij}^2) \quad (3)$$

Instantaneous iso-surfaces of Q-criterion are illustrated for a compressor blade and it is shown that a horse-shoe vortex is formed at the trailing edge of the compressor blade using these contours. Three types of vortices have been identified in this; Induced vortex, Leakage Vortex and Separation vortex [58] .

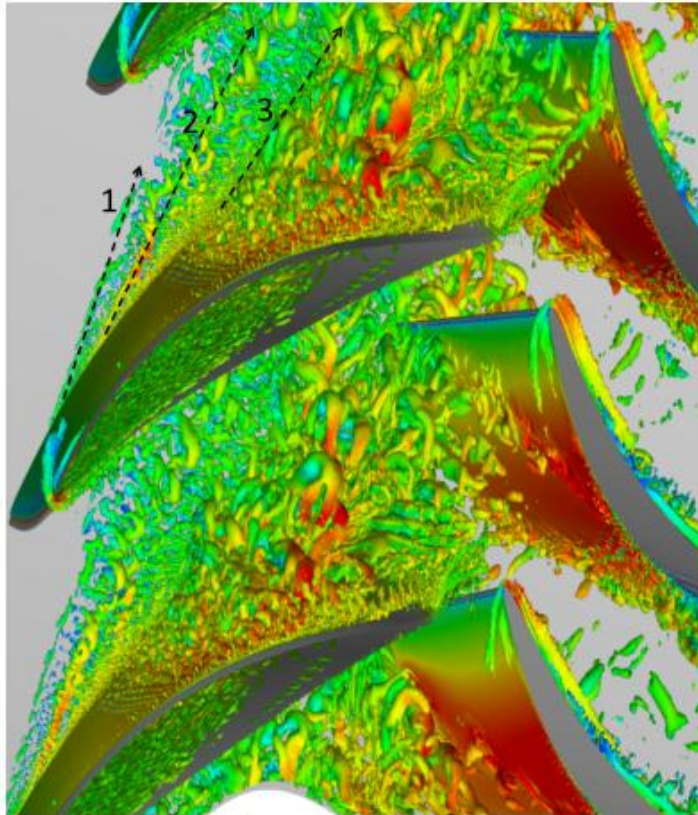


Figure 2.6 – Tip vortices illustration using iso surfaces of Q-Criterion [58]

The horse shoe vortex formation is also identified in another work by using streamlines closer to the hub of a ventilating fan blade. This horse shoe vortex is found to be arising due to the local bluntness of the blade closer to the hub [59].

Helicity contours have been used to identify tip leakage vortices, successfully in previous research work [59].

The transition from laminar to turbulent flow on a rotating rotor blade on the suction side of the blade has been successfully identified using an iso surface of vorticity colored by axial momentum in previous work [60].

Iso surfaces of Q criterion have been used successfully to identify tip vortex generation of a rotating axial rotor, in previous work. The production of tip leakage and tip gap vortex has been successfully identified using these contours [52].

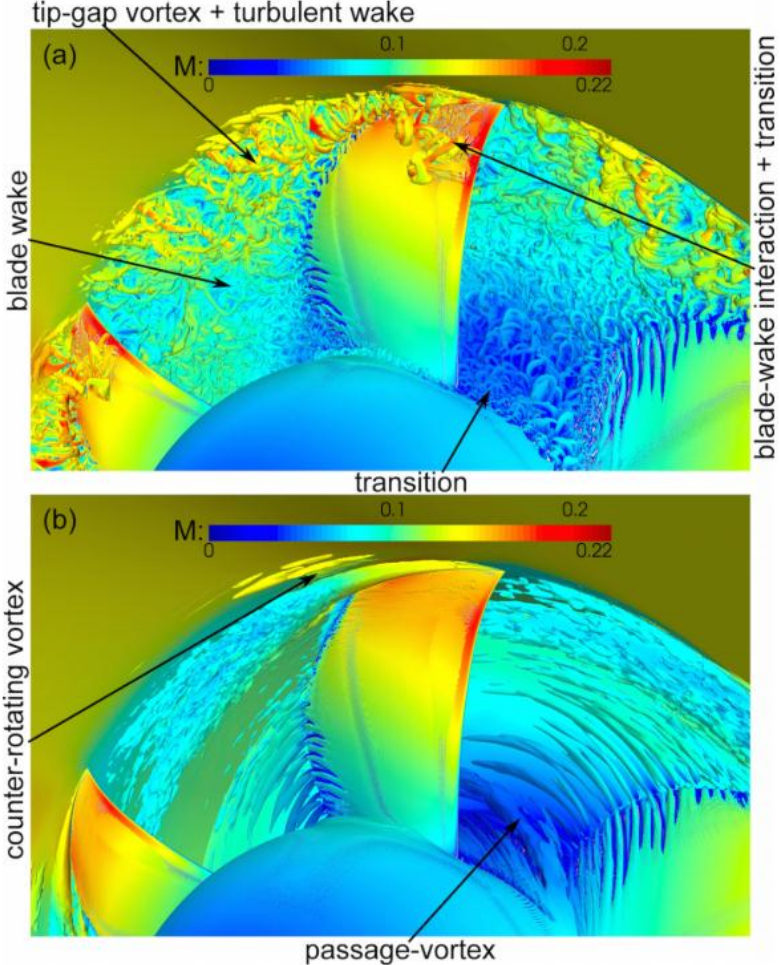


Figure 2.7 – Vortex identification using Q criterion [52]

3. METHODOLOGY

For the completion of two analyses stated in chapter 1 above, two CFD cases were setup. The same setup was evaluated experimentally, in order to validate the two cases. For this analysis, as the test case, USHA – Atom EX model ceiling fan was selected. It is a thin blade fan with rotor diameter of 1400 mm, hub diameter of 190 mm and blade thickness of 1.2 mm. The blades had a taper of 126 mm at the root to 105 mm at the tip. The blades were bent approximately 11° along their spanwise direction at 66% of the chord length. The blades comprise of a pitch angle of approximately 4° . The blades have been manufactured using aluminum sheet metal consisting of a blade area of approximately 680cm^2 .

3.1 Experimental Analysis

3.1.1 Experimental Facility

All experimental work was performed at the ceiling fan test laboratory at the Sri Lanka Standards Institution (SLSI). This laboratory contains test setup for measuring ceiling fan performance as per SLS 1600:2011 Standard.

3.1.2 Experimental Setup

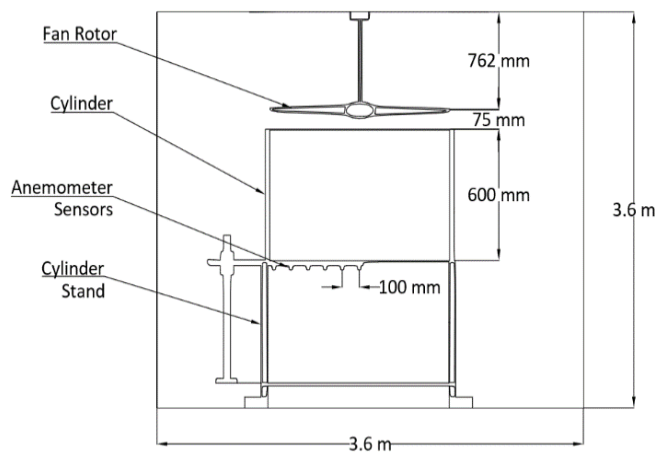


Figure 3.1 - Standard test chamber setup [8]

For the accurate measurement of air velocities, the testing was performed in an enclosed room with close to no airflow interactions. No airflow transfer with surrounding is present. The room is kept empty except for the test barrel and the velocity measuring probes. A cylinder of the same

diameter as the fan was present 75mm underneath the plane of rotation of the fan extending for 600mm, as per the testing standard. The room dimensions were 3600mm x 3600mm x 3000mm (LxWxH). The fan was suspended 760mm below the ceiling. This is shown in the diagram above.

For the data acquisition, Hot Wire Anemometers were used. As shown in figure 3.1, they are placed just below the lowest point of the cylinder. 8 Anemometer sensors were placed in 100mm intervals. The first sensor was placed just below the wall of the cylinder and the final sensor extends to the center of the fan, as shown in figure 3.2.



Figure 3.2 – Test chamber containing the cylinder and the placement of anemometer sensors

The fan is placed in the chamber making sure that it is leveled correctly. The fan was mounted to a rigid hook to minimise any vibrations or oscillations which might arise when the fan is rotating.

3.1.3 Instrumentation

The instruments which were used in the experimental data collection phase are described in detail in this section. The data was acquired through a Data Acquisition Card in the laboratory and was received in electronic spreadsheet format. The data acquired were the velocity readings and room temperature from a temperature probe.

Anemometers

All velocity data was collected by a series of 8 Degree Controls UAS1500XS hotwire anemometer probes. These have been fitted to a stand which can be rotated freely. The vertical position of these probes was fixed and was just below the lowest position of the cylinder. These were interfaced with the DAQ using USB connectors. The anemometer probes were of accuracy of 0.025ms^{-1} in the operating temperature range of $15\text{-}35^{\circ}\text{C}$, without the requirement of any temperature compensation. The measurement range is 0.15ms^{-1} to 20ms^{-1} .

Temperature Probe

The room temperature of the test chamber was recorded by using a Degree Controls UTS1000 Thermocouple. This was also recorded in the electronic spreadsheet via the DAQ card. The measurement range of this thermocouple was -50°C to 250°C with an accuracy of $\pm 1.5^{\circ}\text{C}$.

Data Acquisition Card

The data acquisition card used in this experiment for the data collection was Degree Controls $^{\circ}\text{C}$ Port1200, which was a 12 port Data Acquisition Instrument with USB interface. This was specifically designed for air velocity and temperature data collection. The operating temperature range was 0°C to 70°C and the reading accuracy was $\pm 5\%$.

Tachometer

For the measurement of rotational velocity of the ceiling fan, a hand held type laser tachometer was used. The measurement range of this tachometer was 2-9999RPM and the resolution was 0.02RPM.



Figure 3.3 - Anemometers probe and DAQ card

Digital Power Meter

In order to measure the power consumption per each regulator setting and the power factor, a YOKOGAWA WT310E digital power meter was used. The power consumption was given in watts and the power factor was also displayed in this instrument.



Figure 3.4 – Digital Power Meter

3.1.4 Test Procedures

Data from the velocity and temperature probes were recorded in the computer in the test laboratory. This data collection was performed by Degree Controls AccuTrac data analysis software. The data collection resolution is 2 seconds. The data from the digital power meter and the handheld tachometer were manually recorded per each regulator setting. For the analysis, all the data was entered into one database and calculations were performed computationally.

3.1.5 Experimental Procedure

Rotor Speed Measurement

The rotational speed of the fan was measured by using a handheld laser tachometer. A reflective paper was attached to the hub of the fan in order to reflect the laser beam of the tachometer. Starting from the regulator setting one, the fan was set to each regulator setting and was allowed to reach a stable speed for a few minutes. Once the rotational speed of the fan was stable, the rotational speed of the fan was measured using the laser tachometer. Three readings were taken for each measurement and the average value of these readings were calculated in order to minimise the error.

Air Velocity Measurement

As per the SLS 1600 standard, the air velocity was measured in a plane just below the lowest point of the cylinder, 675mm below the plane of the rotation of the fan, allowing the measurement of velocity in the cylinder plane. The hotwire anemometers were fixed on a stand which was supported by a beam directly below the center of the hub of the fan, reducing the amount of obstructions caused to the air flow. This stand can be rotated allowing readings to be taken at multiple points. As mentioned previously, both the diameter of the fan and the cylinder was 1400mm resulting in 700mm half span length. Eight anemometer sensors were fixed on an arm connected to the support and were placed at intervals of 100mm, starting from the center of the fan which in turn covers the half span of the fan. The readings were taken at 3 vertical planes extending from the center of the fan 120° apart from each other.



Figure 3.5 – Placement of the Anemometers

The readings were taken for each regulator setting starting from regulator position 1. Before taking the readings, the fan was allowed to run-in for a period of 60 minutes. Once the fan was at a stable rotation speed and velocity readings were stable, the data logging was done. No equipment or persons were kept in the test chamber other than the test equipment when performing testing. Before taking readings, the fan was allowed to rotate for 5 minutes at the selected regulator setting, in order to reach stable conditions and to allow any unstable transient fluctuations. Readings were taken for two minutes at each regulator setting at 2 second intervals, accounting to 60 readings at each regulator setting per anemometer sensor. This amounts to 1440 readings per regulator setting.

3.1.6 Derived Data Definition

Based on the measured data, following parameters were derived.

Power Correction

The standard conditions for the experimental testing of ceiling fans was defined as 27⁰C and 101.325 kPa. When the test conditions were varied from these, a correction factor was required to be applied. Corrected pressure was defined as [8]

$$P = P_0 \times \frac{p}{p_0} \times \frac{T_0}{T} \quad (4)$$

Where,

- P – Measure power consumption
- P_0 – Power consumption at standard conditions
- p - Ambient pressure at test conditions
- p_0 - Ambient pressure at standard conditions
- T - Temperature at test conditions
- T_0 - Temperature at standard conditions

Total Air Delivery (Q)

The total flow rate of the fan was calculated by dividing the area swept by the fan in to 8 annulus and multiplying the mean velocity in the annuli by the area of the corresponding annuli [8].

$$Q = \int_{r=0}^R V(2\pi dr) = 2\pi [\sum_{j=1}^M V_j r_j] \Delta r \quad (5)$$

Where,

- M – Number of measuring points (M=8 for 1400mm diameter fan)
- r - Mean radius of the annuli (m)
- Δr - Width of the annuli (0.1m)

Service Value (SV)

The service value was defined as the flow rate per unit electric power input [8].

$$SV = \frac{Q}{P_{Elect}} \quad (6)$$

Where,

- Q – Air flow rate ($m^3 min^{-1}$)
- P_{Elect} – Electrical power input (W)

Average Service Value (\overline{SV})

Average service value was defined as the arithmetic mean of the service values related to different regulator settings [8].

$$\overline{SV} = \frac{\sum_{i=1}^N SV_i}{N} \quad (7)$$

Where,

SV – Service value

N - Number of regulator settings

Marks for Service Value

$$SV_M = \frac{\overline{SV}}{SV^*} \times 100 \quad (8)$$

Where [8],

$$SV^* = 7.2 \text{ m}^3 \text{ min}^{-1} \text{ W}^{-1}$$

Geometric Incremental Flow Rate ($\Delta\overline{Q}$)

Geometrical Incremental Flow Rate was a representation of performance in terms of higher amount of flow rate elements and higher degree of uniformity, in flow rate elements [8].

$$\Delta\overline{Q} = [\prod_{i=1}^{N-1} (Q_{i+1} - Q_i)]^{\frac{1}{N-1}} \quad (9)$$

Where,

Q_i – Flow rate in i^{th} regulator setting

Marks for Incremental Flow Rate (ΔQ_M)

$$\begin{aligned} \Delta Q_M &= \frac{\Delta\overline{Q}}{\Delta Q^*} \times 100; \quad 0 \leq \Delta Q \leq \Delta Q^* \\ &= 100; \quad \Delta\overline{Q} > \Delta Q^* \end{aligned} \quad (10)$$

Average Power Factor

Power factor was defined as the ratio between real and apparent power and the average power factor was the average value of power factors of all regulator settings of a particular fan in consideration [8].

$$\overline{PF} = \frac{\sum_{i=1}^N PF_i}{N} \quad (11)$$

Where,

PF_i – Power factor at the i^{th} regulator setting

Marks for power factor (PF_M)

$$PF_M = 100 \times \left[\frac{\overline{PF} - PF^*}{1 - PF^*} \right]; \quad \overline{PF} > PF^* \quad (12)$$
$$= 0 \quad \overline{PF} \leq PF^*$$

Performance Grading (PG)

Performance grading was determined considering the effect of each performance index and by calculating a weighted average of the values. This is expressed below [8].

$$PG = 0.8 \times SV_M + 0.1 \times \Delta Q_M + 0.1 \times PF_M \quad (13)$$

3.2 Computational Modeling

Computational modeling has been popular from the late 20th century due to the convenience and cost effectiveness of performing acceptable analyses of fluid models. In the recent past, the computational power of accessible resources has increased drastically. This has caused this field to expand even more and is becoming more prevalent in research institutions and industry. Further, this improvement of computational power has led to more accurate results due to the use of finer meshes and higher number of iterations.

In this research Ansys 18.1 Fluent Commercial, which is a common CFD programming tool is used for both the analysis of the effect of ceiling fan test chamber geometry on the performance measurement of ceiling fans and the flow field characteristics around a rotating ceiling fan blades.

The flow physics analysis was done by using LES in transient condition using sliding mesh technique while the analysis of effect of the test chamber geometry was done by using RANS simulations in steady state condition using MRF technique, as stated previously.

For both the cases, initially the geometry was generated equally, and the mesh generation and setup were done for each case depending on LES or RANS method. A finer mesh was generated for the LES case and a coarser mesh was generated for the RANS case considering the computational cost and the results required.

3.2.1 Model of the Fan

The fan domain needed to be modeled in a CAD program before the implementation in the CFD software. The solid model of the fan was created in Solidworks 2018. The dimensions of fan components were measured with accuracy of $\pm 1\text{mm}$. Minor features such as small edges, rivet heads, screws, and some chamfers and fillets were ignored to prevent complications in meshing and calculations.

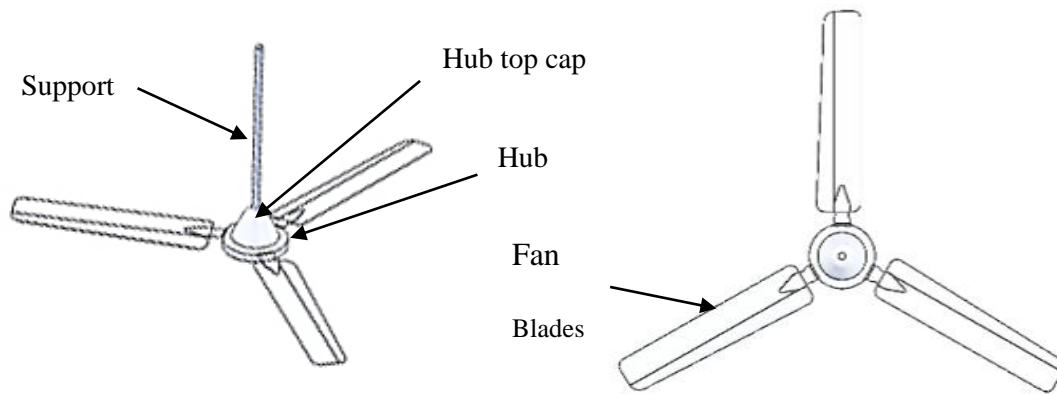


Figure 3.6 – 3D Model of the ceiling Fan

The geometrical model was created in actual scale. It was modeled according to SLS standard 814 for testing of ceiling fans. It contained the ceiling fan inside of a confined room of 3600x3600x3000 mm (WxDxH) and a drum placed 75 mm below the plan of the rotation of the fan as per the standard. The distance from fan to the ceiling was 762 mm. For the analysis of effect of test chamber geometry on the performance measurement of the fan, these geometry parameters were changed accordingly and it was mentioned in detail in the respective section below.

The Solidworks model was then imported to Ansys Fluent Design Modeler to proceed with the CFD modeling. The domain was subdivided into 11 volumes to obtain a mesh with least number of cells with fine elements in the required sections. The origin of the coordinate system was placed at the center of the hub of the fan, in the plane of rotation.

The mesh was designed such that the neighboring volumes are in agreement with each other in each section. The mesh generation for each volume will be discussed in more detail in the following section. The volumes were separated by interior planes, which were invisible to the flow and only serve as a function for mesh generation. The simulation domain is shown in Figure 3.8.

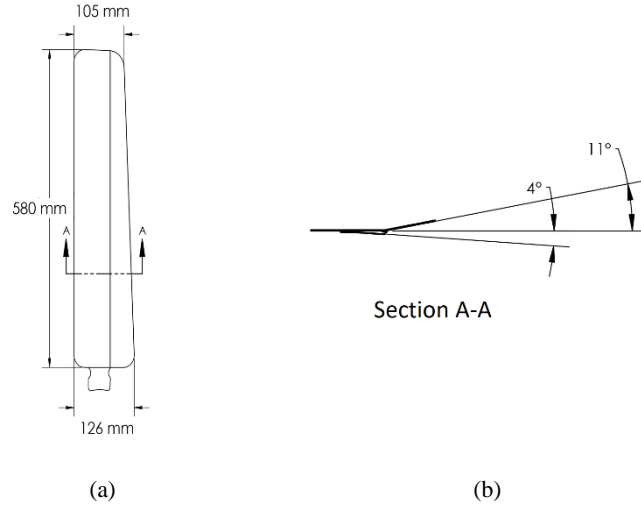


Figure 3.7 – Fan rotor dimensions
 (a) – Plan View
 (b) – Rotor pitch across A-A

A cylindrical zone containing the fan is separated in this, in order to specify a rotating zone. Another cylindrical zone containing the hub top cap of the fan removed from the top center section, since the hub top cap is stationary. This is shown in figures 5.8 and 5.9.

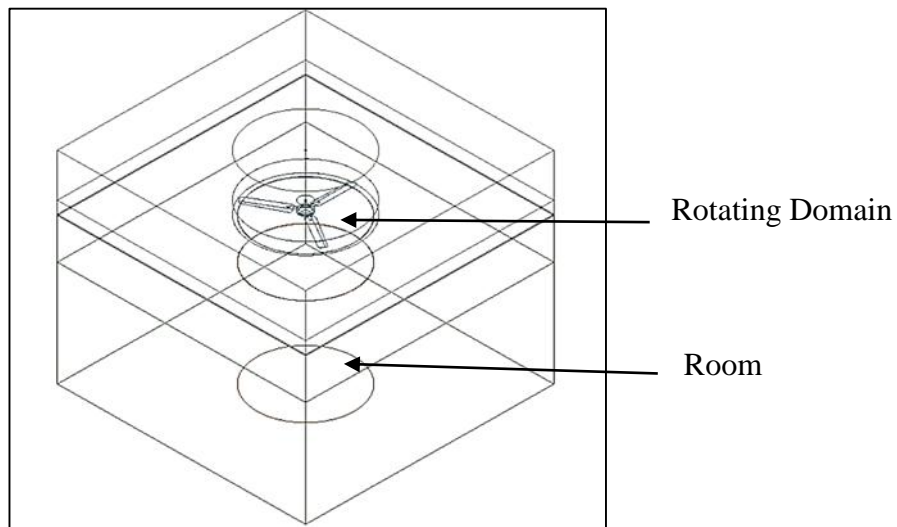


Figure 3.8 – CFD domain

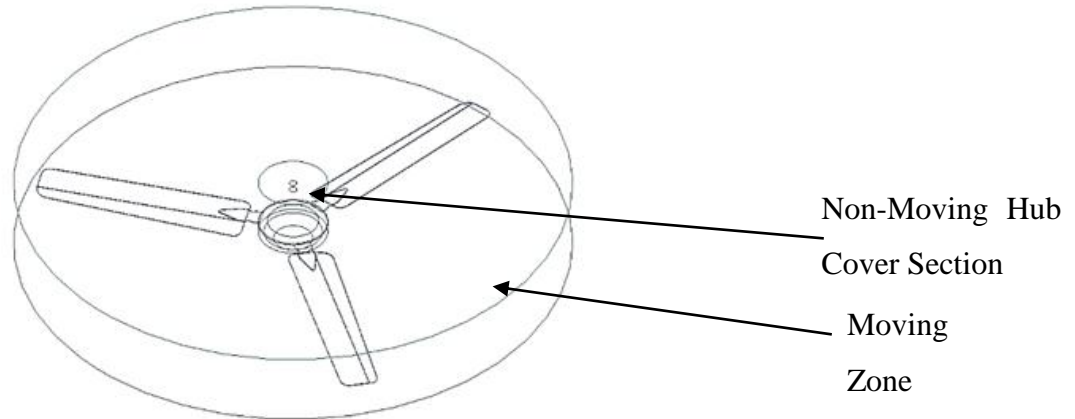


Figure 3.9 – Close view of moving section

3.2.2 Mesh Generation

The mesh generation was done using ANSYS mesher. All of the faces in the computational domain was named and sizing was given as required. The moving zone was meshed using unstructured patch conforming tetrahedrons method and stationary zones were meshed using structured hexa method except, for the hub top cover region, which was also tetrahedral. In order to obtain a structured mesh, face meshing was done and it was swept across the considered volume. Meshing was done by selective meshing technique to obtain a conformal mesh. Structured hexa mesh was used as much as possible to reduce the number of elements, which would in turn reduce the computational time and to increase the accuracy of the calculations.

The moving zone was meshed with much smaller elements than the non-moving zone. Further, the element size was reduced additionally by body of influence technique near the fan blades in order to capture more sensitive details near the fan blades. The rest of the volumes were comparatively coarsely meshed. The flow velocity in these volumes was low and had minimal disturbances to the flow. Therefore, a coarser mesh allowed the flow to be solved to a high enough resolution while not demanding too much computational time.

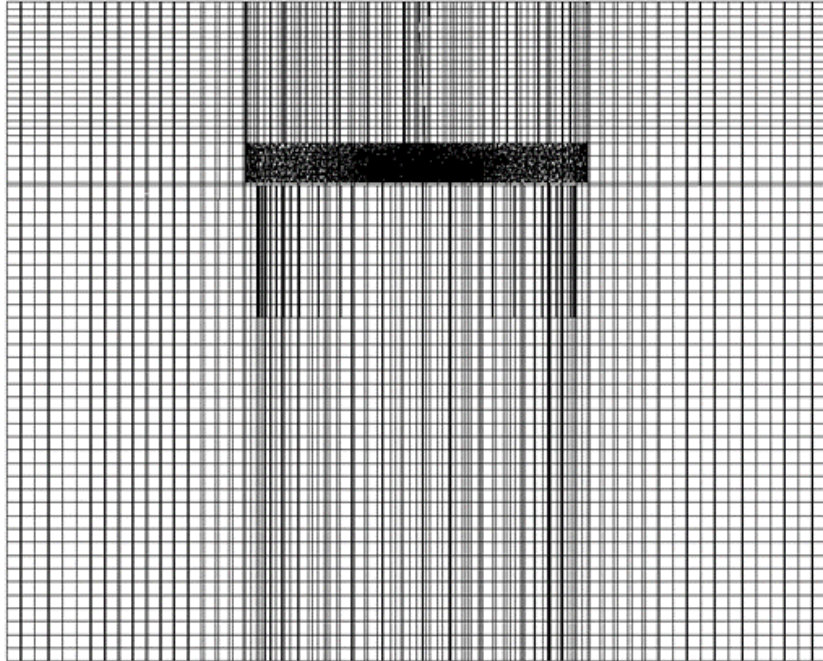


Figure 3.10 - Cross Sectional view of the mesh

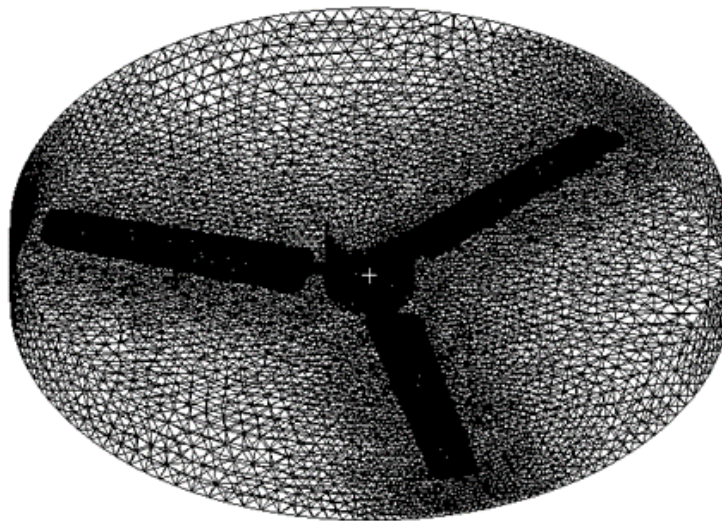


Figure 3.11 – Mesh in the moving region

3.2.3 Turbulence Modeling

For this research, as described previously, a steady state modeler was used in the analysis of effect of test chamber geometry on the flow field generated by the fan, and a transient simulation was used in the flow physics analysis in order to obtain a more thorough understanding of the flow field around the fan. For the turbulence modeling, several models were evaluated.

SA model is a one equation transport model used for turbulence modeling RANS simulations. This model is compatible of any grid structure and it is shown that this equation yields acceptable results for indoor simulations [43]. Further it is shown in previous research that this model yields results closer to experimental results for a similar case [41].

In this model the turbulent eddy viscosity is given by [43],

$$v_t = C k^{1/2} l \quad (14)$$

Where v_t is the eddy viscosity, l is the turbulence length scale, k is turbulent kinetic energy and C is a constant coefficient.

The KE model is a two-equation transport model used for turbulence modeling in RANS simulations. These two equation models are expected to give superior results than one equation models, but the results would depend on the specific case [44]. The KE model is used widely for indoor airflow simulations. Though the standard KE model is mainly applicable to high Re flows it can be applied for low Re flows with wall functions to model flows in the vicinity of walls.

In this model the turbulent eddy viscosity is given by [43],

$$v_t = C_\mu \frac{k^2}{\epsilon} \quad (15)$$

Where k is the turbulence kinetic energy, ϵ is the dissipation rate of turbulence energy, and $C_\mu = 0.09$ is an empirical constant.

The Renormalization Group KE model (RNG KE) has also been used widely for indoor flow simulations. It has been validated for air distributions in an office space and a classroom and it is shown that the results are in good agreement with experimental results. [61]

The KW model is another two-equation transport model. This is known to give improved results than KE model in adverse pressure flows. This model has also been used for indoor air distribution simulations and is known to give good results. [43]

In Large eddy simulation, Large eddies are solved directly using transient DNS calculation. Small eddies are filtered and modeled using a subgrid-scale (SGS) model. LES method Requires 3-D transient modeling and spatial and temporal resolution of scales in “inertial subrange”. LES method has far better accuracy compared to any RANS model [39]. It falls between RANS and DNS methods. LES method requires more computing power than RANS methods. But in order to obtain a more accurate solution, LES was used in this research for the physics analysis around the fan blades.

Depending on this study, the flow physics analysis around the fan blade is done using LES method. For the analysis of the effect of the test chamber geometry on the flow field generated by the ceiling, several RANS models are evaluated, and analysis was done using the model yielding results closest to experimentally measured values.

3.2.4 Solver Setup

There are two solvers that are used for solving the energy, continuity, and momentum equations: Pressure-based and density-based solvers. The pressure-based solver is used when the flow is incompressible or mildly compressible while the density-based solver is used when flow is compressible. Density based solver is computationally expensive than pressure-based solvers. Since the flow in a ceiling fan is low speed and has a low Mach number (<0.01), it is assumed to be incompressible and pressure-based solver is used in this research.

Pressure based solver can be used either in segregated or coupled manner. Coupled scheme is said to be more robust and it is advantageous to use coupled solver instead of a segregated solver in steady state problems. Further, for transient flows, a coupled solver is recommended when the time steps are sufficiently large or when the mesh is of not perfect quality [23]. Therefore, in this research pressure based coupled solver has been utilised for both steady and transient simulations.

3.2.5 Simulation of Motion of Blades

For the simulation of motion of an object, mainly three approaches can be used. Namely, Moving Reference Frame (MRF) method, Sliding mesh method and dynamic mesh method. Out of these three methods, the dynamic mesh method uses automatic meshing as motion occurs to update the mesh, and it cannot be guaranteed a good quality mesh can be obtained for complex geometries. Therefore, in this research, MRF and Sliding Mesh methods have been used.

Sliding Mesh Method

For the simulation of the rotation of the fan blades in the transient condition, the sliding mesh method, which is a form of a moving mesh was used. In the sliding mesh model, the nodes of the mesh move rigidly in the dynamic zone. The cells between dynamic and static zones are connected through non-conformal interfaces. Sliding mesh model is a transient state model in which it updates each timestep and provide solutions with each update. In each time step as the mesh motion is updated in time, the interfaces are also updated. In this research, the zone containing the fan blades were allowed to move (rotate) with respect to the stationary zone. In sliding mesh model, any mesh interface that does not remain in contact with each other is treated as a wall [39]. Therefore, the interfaces were made circular (cylindrical) to make it remain in contact as the mesh was updated. The interfaces at the fan blades were treated as walls. This caused the simulation to look like the fan blades were rotating physically.

Equations for sliding mesh model

Since the rotating zone is in motion in respect to the stationary zone, vector quantities must be treated at the interfaces between the two zones. Scalar quantities such as pressure, temperature and density are same in both the regions and no changes need to be done mathematically. For this purpose, to treat the vector quantities, a moving reference frame is employed in the sliding mesh model [62]. The transformation from fluid velocities in the stationary to the rotating reference frame are given by,

$$U_r = U - \omega \times r \quad (16)$$

The continuity equation is given by

$$\frac{\partial \rho}{\partial t} + \nabla \cdot (\rho U_r) = 0 \quad (17)$$

The Momentum equation is given by

$$\frac{\partial}{\partial t} (\rho u) + \nabla \cdot (\rho u_r u) + \rho(\omega \times u) = -\nabla \rho + \nabla \cdot \left[\mu(\nabla u + \nabla u^T) - \frac{2}{3} \mu(\nabla \cdot u) \right] + F \quad (18)$$

Where,

\vec{v}_r –Relative velocity (velocity viewed from moving frame)

U – Absolute velocity

\vec{u}_r –Velocity of moving frame relative to the inertia reference frame

$\vec{\omega}$ – Angular velocity relative to stationery (inertia) reference frame

r – Position vector from the origin of the rotating frame

\vec{F} – External body forces

ρ – Density

MRF Method

In this method, a moving body in inertial frame was made stationary with respect to a moving reference frame. This is used in steady rotating problems widely. This method is proven to provide acceptable results. In steady state problems, this method provides time averaged solutions. [39]

Equations for moving reference frame model

Similar to sliding mesh model, vector quantities were treated and scalar quantities were passed at the interfaces between moving and non-moving regions. The equations for moving reference frame can be given as [41] [39],

For Velocities,

$$U_r = U - \omega \times r \quad (19)$$

The continuity equation is given by

$$\frac{\partial}{\partial t} \rho E + \nabla \cdot (\rho \vec{v}_r H + p \vec{u}_r) = \nabla \cdot (k \nabla T + \vec{t} \cdot \vec{v}) + S_h \quad (20)$$

The Momentum equation is given by

$$\frac{\partial \rho \vec{v}_r}{\partial t} + \nabla \cdot (\rho \vec{v}_r \vec{v}_r) + \rho [\vec{\omega} \times (\vec{v} - \vec{v}_t)] = -\nabla p + \nabla \cdot \vec{\bar{\tau}} + \vec{F} \quad (21)$$

Where,

\vec{v}_r –Relative velocity (velocity viewed from moving frame)

U – Absolute velocity

\vec{u}_r –Velocity of moving frame relative to the inertia reference frame

\vec{v}_t - Translational frame velocity

$\vec{\omega}$ – Angular velocity relative to stationery (inertia) reference frame

r – Position vector from the origin of the rotating frame

$\vec{\bar{\tau}}$ – The total stress tensor

S_h - Source added

E- Energy

\vec{F} – External body forces

H- Relative total enthalpy

ρ – Density

p – Static Pressure

Mesh Interfaces

For the movement of the flow properties from the rotating zone to the stationary zone, mesh interfaces were introduced at the boundary of the two zones. These were created by connecting the boundary of stationary zone with the rotating zone. The rotating zone was selected as the target interface.

3.2.6 Boundary Conditions

All of the boundaries in the interior of the stationary section, created due to slicing of the fluid volume were made conformal by using share topology technique. The boundaries were then invisible to the flow. Other boundaries such as the boundaries of the room and drum were made adiabatic walls. In the rotating section, the blades of the fans were also made as walls. The air volume was set to 28⁰C temperature.

3.2.7 Cell zone conditions

The rotating zone of the fluid domain was given mesh motion as per the sliding mesh and MRF models to generate the rotation of the fluid. It was given rpm values corresponding to the selected regulator setting in the clockwise direction according to the actual case of operation of the ceiling fan.

3.2.8 Initialization and Calculation

LES Simulation

For the LES Simulation, a precursor RANS Simulation is required for initialization and error minimization. For this purpose, the RNG K-E model with enhanced wall functions were used. The number of iterations were selected depending on the number of elements of each mesh considering the time factor. This RANS simulation was first run on steady state using MRF for the simulation of the rotating fan blades, then was changed to transient simulation using sliding mesh method, midway of the precursor simulation.

Once it was determined that the precursor simulation had been running for a sufficient amount of time, and the solution was stable, the calculation was changed to LES, while using WALE Model for sub grid modeling.

RANS Simulations

For the RANS simulations several turbulence models popularly in use for CFD calculations were evaluated. This simulation was performed on steady state with MRF approach due to time considerations. The calculation was run for sufficient amount of time and the results were taken.

Convergence Criteria

The convergence criteria was used as 0.001 for continuity and momentum.

3.2.9 Analysis of the Effect of Ceiling Fan Test Chamber Geometry on the Performance Measurement of Ceiling Fans

The ceiling fan test chamber geometry is specified differently, in different test standards used by different countries across the world. Further, some of these standards use a cylinder in order to direct the airflow generated from the fan towards the anemometer sensors, as specified before. The placement of this test cylinder and its geometry is defined arbitrarily in these standards. Clear research of these geometry parameters on the performance evaluation is not available.

Therefore, in this research, different geometry parameters of these standards have been evaluated to analyse the effect of the test chamber on the performance evaluation taking namely the United States ANSI 230 standard and SLS 1600:2011 standard as the extreme limits, and the data has been analysed by taking SLSI standard as the base case. The evaluation is performed for 3 rotational speeds corresponding to 1st, 3rd, and 5th regulator setting of the fan.

The parameters evaluated are summarised in Table 5.1 below.

Parameter Evaluated	Variations in mm	Speed (RPM)
Cylinder length	600	129.2
		234.5
		287.2
	750	129.2
		234.5
		287.2
	914	129.2
		234.5
		287.2
Cylinder diameter	1400	129.2
		234.5
		287.2
	1500	129.2
		234.5

		287.2
	1600	129.2
		234.5
		287.2
Gap between cylinder and plane of rotation of fan	75	129.2
		234.5
		287.2
	125	129.2
		234.5
		287.2
	152	129.2
		234.5
		287.2
Room size	3600 x 3600x3000	234.5
	4500x4500x3000	234.5
	6000x6000x3000	234.5

Table 3.1- Parameters evaluated during simulations

4. RESULTS

4.1 Experimental Results

The experiments are performed at the ceiling fan testing laboratory at Sri Lanka Standards Institution (SLSI) as per the method stated in the previous section.

Data from 8 hot wire anemometer sensors and one thermometer is taken from the DAC in a spreadsheet file and the power data from the power analyser and the fan speed from the laser tachometer is manually recorded. The time averaged velocity per anemometer is calculated by time averaging the data set obtained for a period of two minutes and spatially averaging it with data obtained at three anemometer positions, namely 0° , 120° and 240° . The average flow rate is calculated by the anemometer data in order to gain a meaningful understanding.

4.1.1 Assumptions

In the process of acquiring experimental data, following assumptions were made

1. The rotational speed variation caused due to the fluctuations in the supply voltage is negligible.
2. The effects caused due to the vibrations of the rotor of the fan on the flow field is negligible.
3. The ambient pressure in test conditions is equal to the standard pressure

4.1.2 Results

The running RPM of the fan at different regulator settings were also measured following the described method and is given in Table 4.1 below.

Regulator Setting	RPM
1	129.2
2	180.5
3	234.5
4	258.3
5	287.2

Table 4.1 – Measured RPM values

The collected data are averaged in the 3 vertical planes as mentioned above, in order to obtain a spatially discretized solution. The calculated data is depicted in the Figure 4.1.

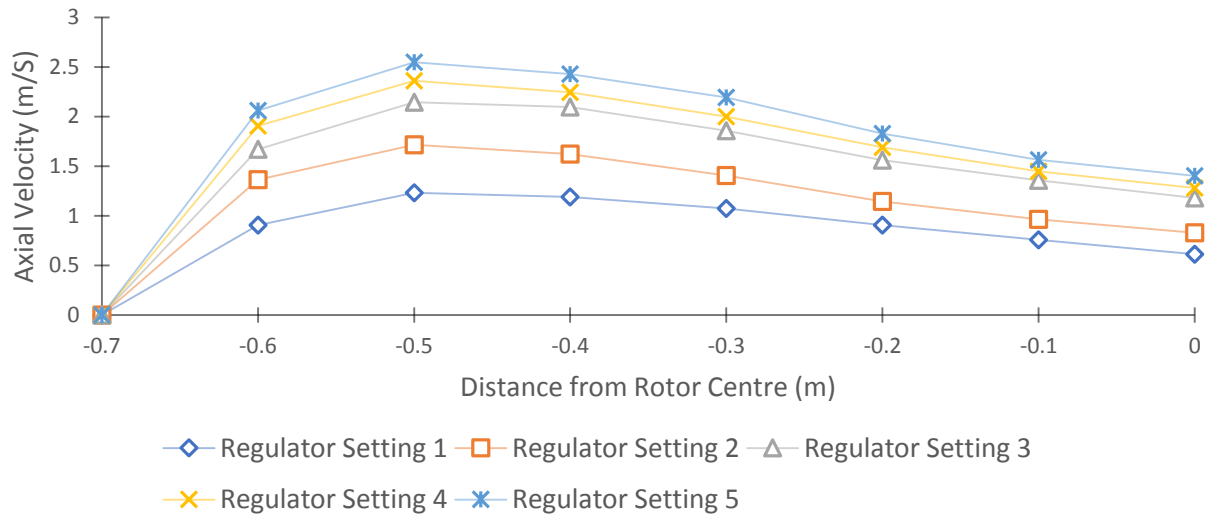


Figure 4.1 – Spatially and time averaged experimental data

The results show that the air velocity is lower near the tip and the hub of the fan. It is minimum near the tip of the blade. Maximum velocity is observed at about 70% of the fan blade. These results are conforming to the results described in similar research [41] [32].

The flow parameters under different RPM values corresponding to regulator settings of the employed ceiling fan are given in the table 4.2.

Regulator Setting	RPM	Maximum air velocity	Power Factor	Input Power (W)	Corrected Power	Mean Flow Delivery (Q)
1	129.2	1.2	0.48	16.7	16.9	94.1
2	180.5	1.7	0.61	27.7	28.0	133.2
3	234.5	2.1	0.76	41.6	42.2	171.2
4	258.3	2.4	0.85	49.6	50.2	189.0
5	287.2	2.5	0.98	60.9	61.7	203.7

Table 4.2 – Flow parameters at different RPMs

It can be observed that as expected the regulator setting one gave the lowest axial velocities and the regulator setting 5 gave the highest axial velocity values. Further, it is evident that the percentage increase of the velocities are decreased when the regulator setting is increased from 1

to 5, as shown in figure 4.2 (b). With the increase of average velocity with the regulator setting, the flow rate is increased as well.

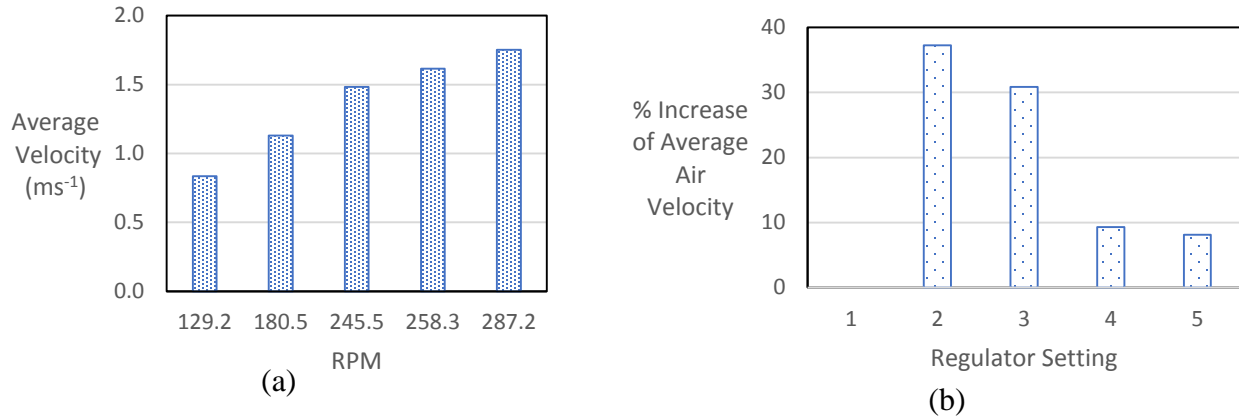


Figure 4.2 – Measured parameters at different regulator settings
 (a) – Variation of average air velocity with regulator setting
 (b) – Percentage increase of average air velocity with regulator setting

4.2 CFD Simulations

Two separate CFD cases were setup to analyse the two cases, analysis of the effect of ceiling fan test chamber geometry on the performance measurement of ceiling fans using RANS simulations and analysis of the flow field characteristics around a rotating ceiling fan blades using LES as mentioned previously and the obtained results of the two cases are detailed in below sections respectively.

4.2.1 Case 1: Analysis of The Effect of Ceiling Fan Test Chamber Geometry on The Performance Measurement of Ceiling Fans

The same experimental setup was simulated with CFD and the results obtained were compared in order to analyse the accuracy of the developed computational model. Axial velocity was obtained at different points along the diameter of the barrel, just below the lowest point of the barrel, similar to the experimental setup. In order to obtain a spatially averaged solution, data was collected in 11 lines equally spaced with each other, spread in an angle of 120⁰ and the average value was taken. No time averaging was required since the simulations were performed at steady state condition. Data was collected in all five regulator settings. The results obtained are depicted in figure 4.3 (a) below.

Mesh Sensitivity Analysis

A sensitivity analysis was performed on the grid resolution in order to establish the mesh independence. Three grids were analysed with different sizes and number of cells, as depicted in Table 4.3 below. The variation of the output velocity along radial direction, averaged velocity and mass flow rate was analysed. It was seen that these parameters do not depend significantly on the grid size at the selected values, though the average velocity of 1.4M mesh was slightly lower than expected values. Based on these data 2.7M mesh was selected for further calculations as it's the most economical mesh that is closest to the experimentally measured values in terms of axial velocity. This is illustrated in Figures 6.3 (a) and (b).

Mesh Size (Millions of Cells)	Average Velocity (ms^{-1})	Mass Flow (kg s^{-1})
1.4	1.31	2.91
2.7	1.36	2.89
3.9	1.34	2.87

Table 4.3- Variation of output with mesh size

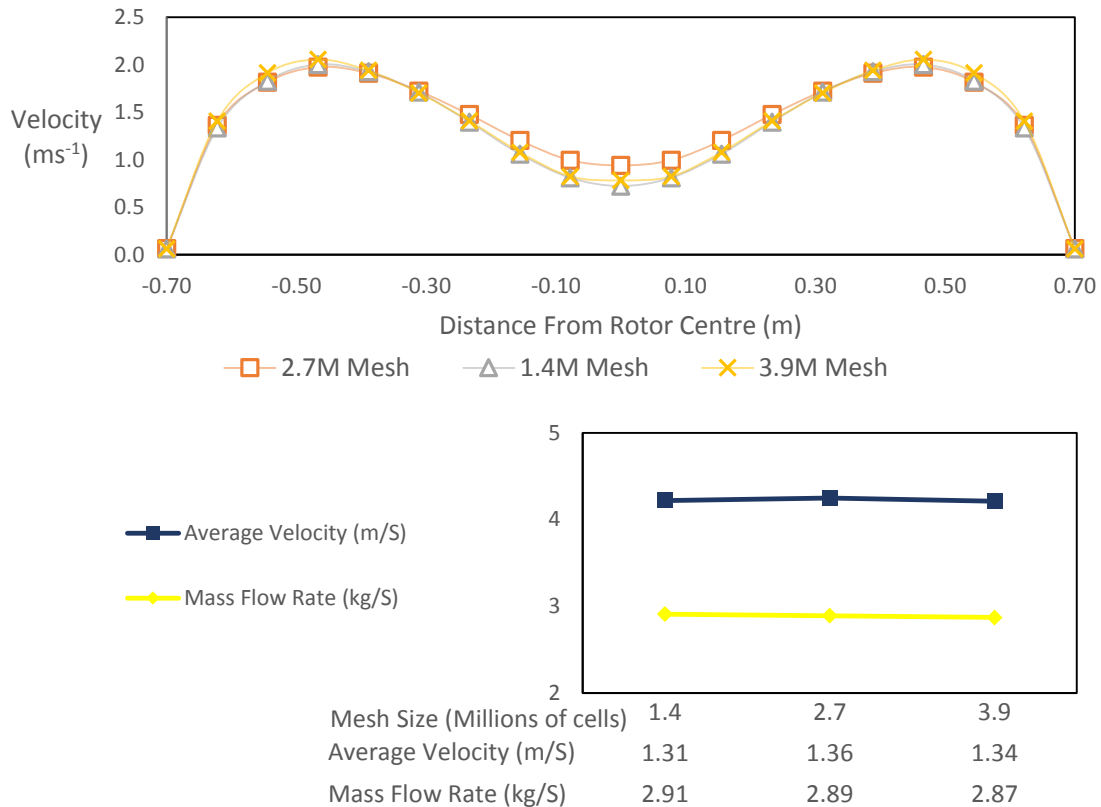


Figure 4.3 – Variation of output parameters with mesh size

(a) – Variation of axial velocity

(b) – Variation of mass flow rate and average velocity with mesh size

Evaluation of Turbulence Models

Using the selected grid, the effect of the turbulence model on the output velocity was evaluated for Standard KE model, RNG KE model, KW model and SA model, at standard rotational speed of 234.5 rpm, which corresponds to regulator setting 3. The obtained results are presented in Figure 4.4 below.

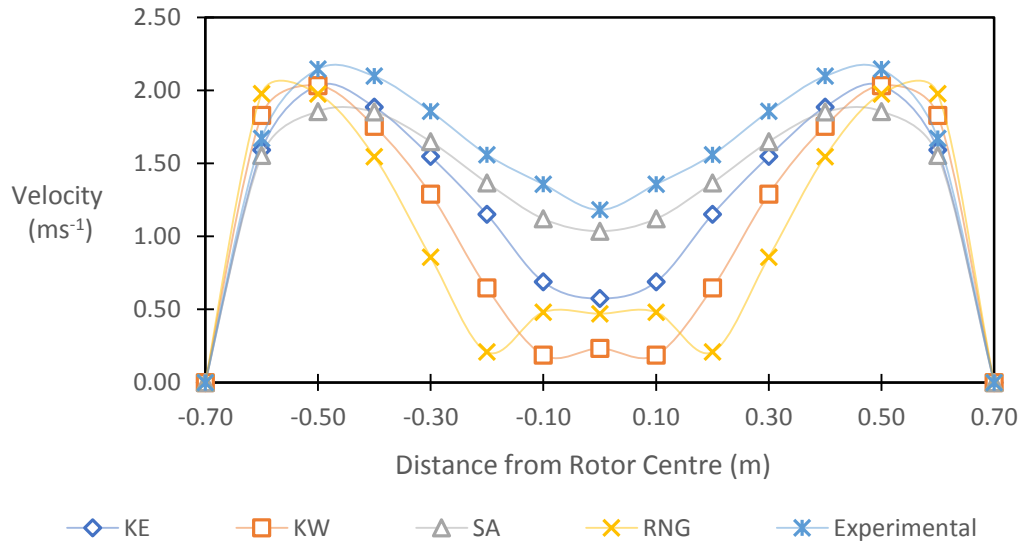


Figure 4.4 – Effect of the turbulence model on the output velocity for different turbulence models

In order to assess the results in each case with experimental data, Normalized root-mean-square deviations (NRMSD) was calculated.

$$NRMSD = \frac{\sqrt{\{\sum_{i=1}^n (V_j - V_0)^2\}/n}}{(V_{j,max} - V_{j,min})} \quad (22)$$

Where,

i = Measured location

n = Number of locations

V_j = Velocity of the considered case

V_0 = Velocity of the case without a test cylinder

	KE	KW	SA	RNG
NRMSD	0.133	0.236	0.070	0.265
%	13.3	23.6	7.0	26.5

Table 4.4 -Calculated RMSD between cases using different turbulence models

Upon comparison of these results, it is seen that SA model predicts velocity values closest to the experimental results. Therefore, this model is further investigated for other RPM values, and the results obtained are presented in Figure 4.5 below.

Validation against experimental data

The predicted results from the CFD simulation of the selected mesh was assessed against experimentally measured values as depicted in Figure 4.5, to determine the accuracy of the CFD setup.

Regulator Setting	NRMSD %
1	4.8
2	5.4
3	7.0
4	7.0
5	9.6

Table 4.5- Calculated NRMSD between simulated case using SA turbulence model and experimentally measured values for the five test cases

The average of RMSD value between simulated case using SA turbulence model and experimentally measured values for the five test cases was calculated as 6.7%. Therefore, it can be verified that SA turbulence model in combination with MRF approach can be used to accurately predict velocity values for the case considered.

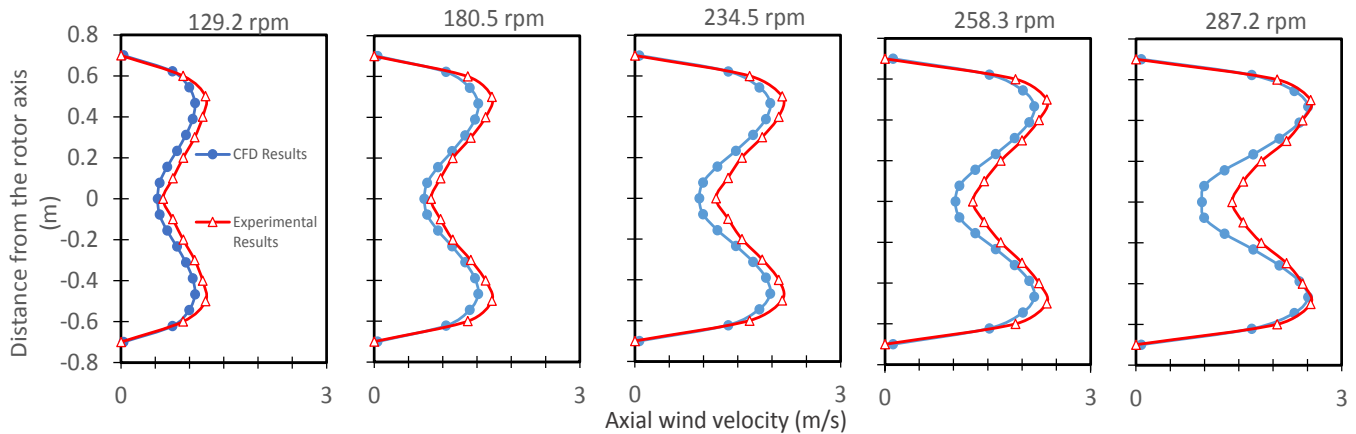


Figure 4.5 – Comparison of axial velocity results of SA model with that of experimental results

This is further verified previous work, which shows that Spalart Allmaras models give superior results close to the experimental results. [41] Therefore, for the RANS simulations, Spalart Allmaras model is selected.

Simulated Data

The simulations are performed for RPM values corresponding to all five regulator settings. The generated data reflected the collected experimental data; the maximum axial velocity was around 0.7R across most RPM values. This is due to the presence of a tip vortex due to the leakage flow at the tip of the blade, which reduces the pressure difference between the top and bottom sides of the blade closer to the blade tip, which in turn reduces the momentum gained by the downward flow from the fan blade closer to the tip leading to a lower flow velocity close to the tip of the blade. This is illustrated in Figure 4.7 (a). The generated velocity contours presented in Figure 4.7 (b) through 4.7 (d) provide a clear understanding of the air velocity distribution inside the chamber, in line with previous similar studies.

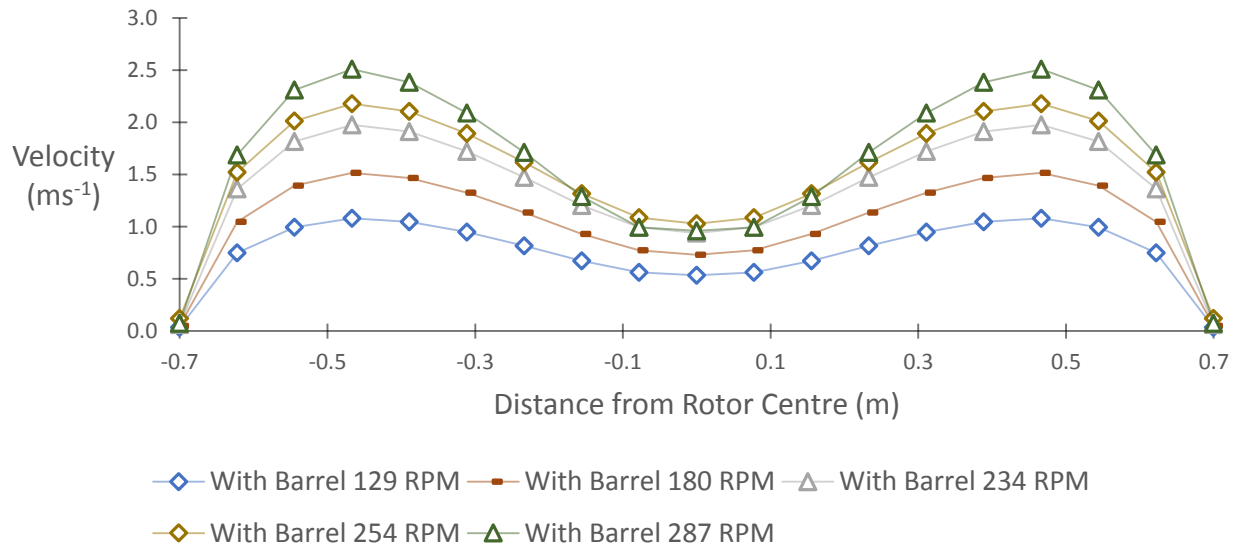


Figure 4.6 – Simulated Results

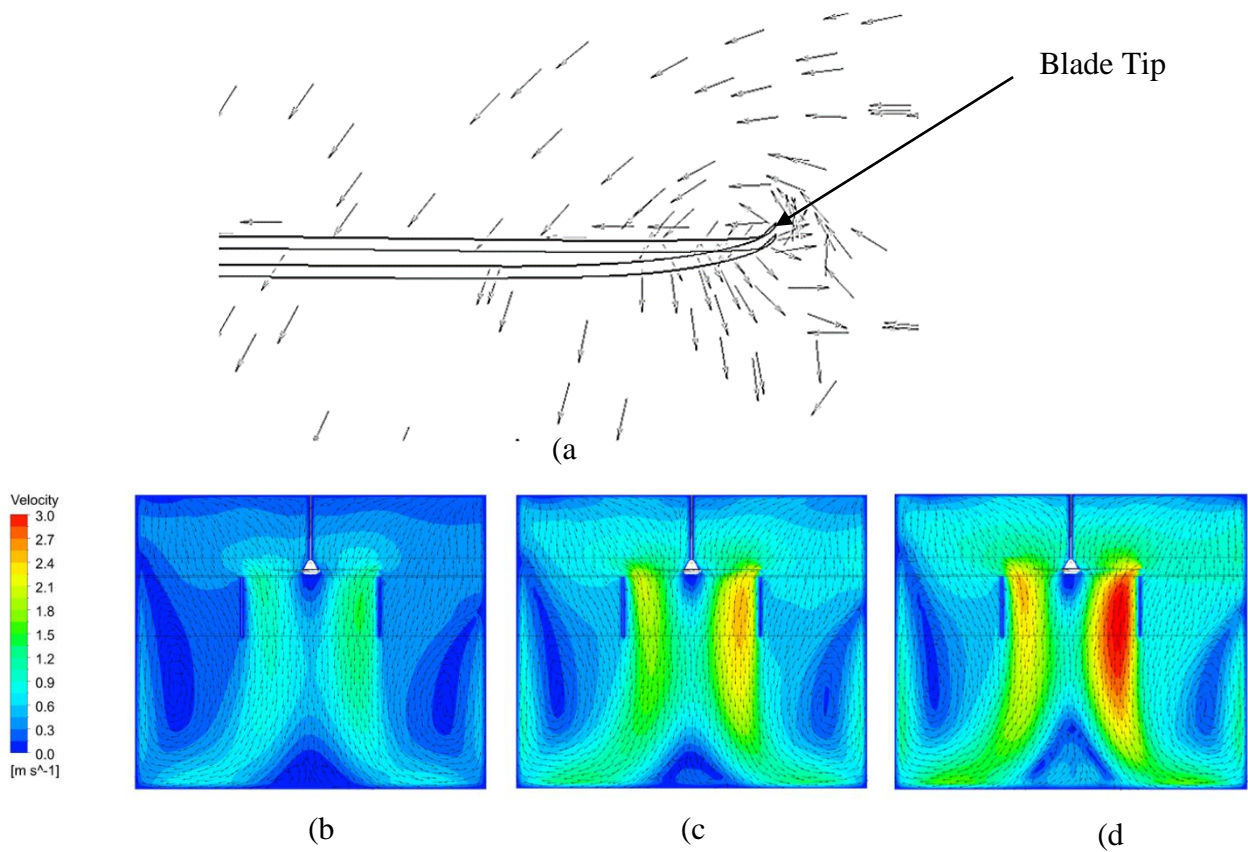


Figure 4.7 – Generated velocity distributions
 (a)– Vertex plot of tip vortices
 (b) – Generated velocity contours in mid plane at 129.2 RPM
 (c) - Generated velocity contours in mid plane at 234.5 RPM
 (d) – Generated velocity contours in mid plane at 287.2 RPM

As stated above, it is seen that the results are acceptable, and analysis can be performed based on these results. Therefore, the for the analysis of the effect of each of these parameters on the efficiency calculation on a ceiling fan is evaluated primarily by the analysing the effect of each of these geometry conditions on the service value and the flow coefficient described above, ultimately analysing the effect on calculation of energy rating described in the same.

Effect of Tested Parameters on the Generated Flow

Initially, the simulation was run in the base case for all five RPM values. Then, the analysis of the effect of test setup geometry on the flow field generated by the fan is performed by evaluating different configuration parameters as specified in methodology section above.

The effect of the test geometry on flow coefficient, flow rate and service value parameters were analysed and is presented in the following section.

Effect of the Gap Between Test Cylinder and Plane of Rotation of Fan

The effect of the gap between the test cylinder and the plane of rotation of the fan on the flow field generated was analysed at three configurations; Gap at 75 mm; corresponding to SLS 1600:2011 standard, Gap at 125 mm, Gap at 152 mm; corresponding to ANSI 230 standard. This analysis was carried out at Three RPM values corresponding to three regulator settings as specified previously, and the results are illustrated below.

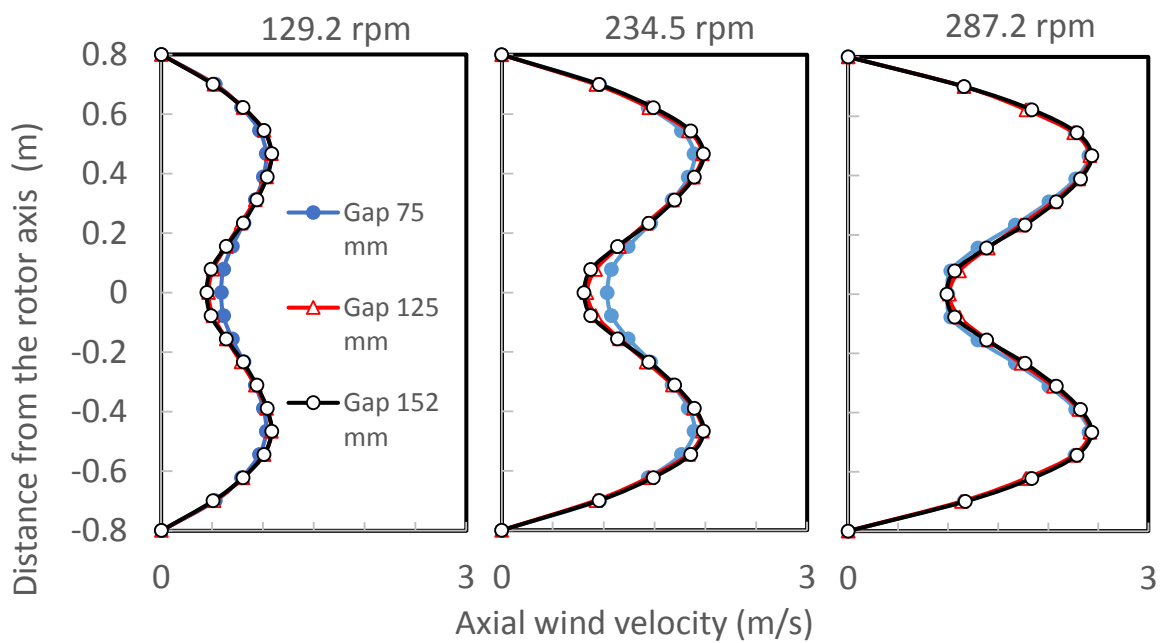


Figure 4.8 - Effect of the gap between the plane of rotation of the fan and the test cylinder

Effect of the Height of the Test Cylinder

The evaluation of the effect caused by the height of the test cylinder used in test setup on the measured parameters was evaluated at three configurations, at three RPM values; similar to the above case. The three configurations were Cylinder height at 600 mm; corresponding to SLS 1600:2011 standard, Cylinder height at 750 mm, Cylinder height at 914 mm; corresponding to ANSI 230 standard. The obtained results are illustrated below.

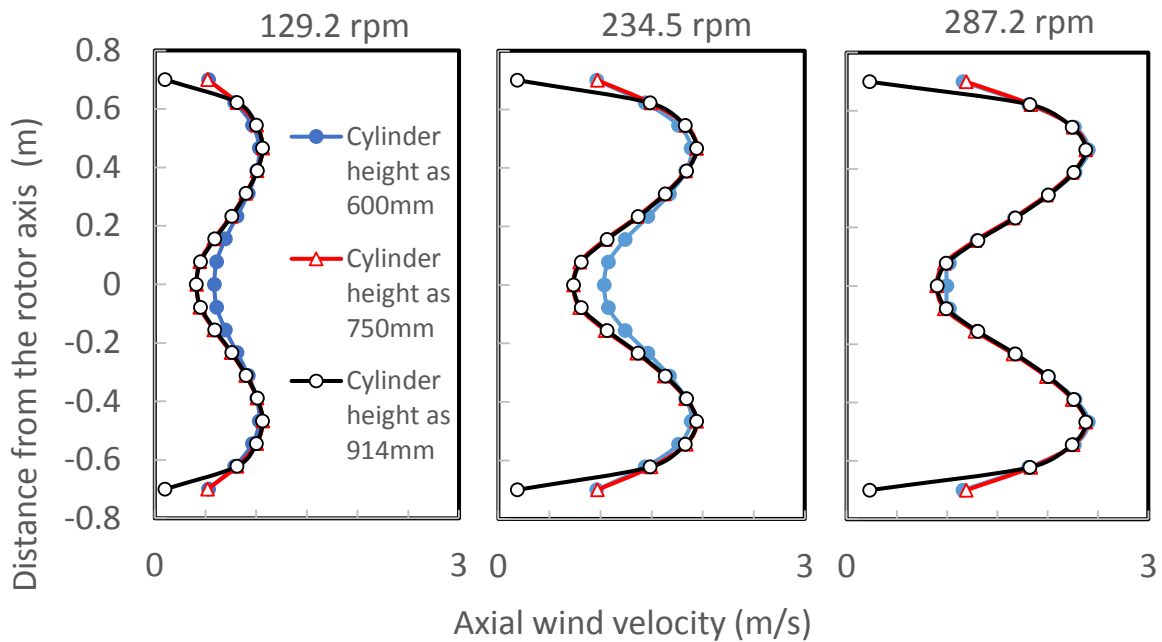


Figure 4.9- Effect of height of the test cylinder

Effect of the Diameter of the Test Cylinder

Similar to the above cases, the effect that the diameter of the test cylinder has on the measured parameters were also evaluated. This was also done at three RPM values as specified above. The obtained results are illustrated in Figure 4.10 below.

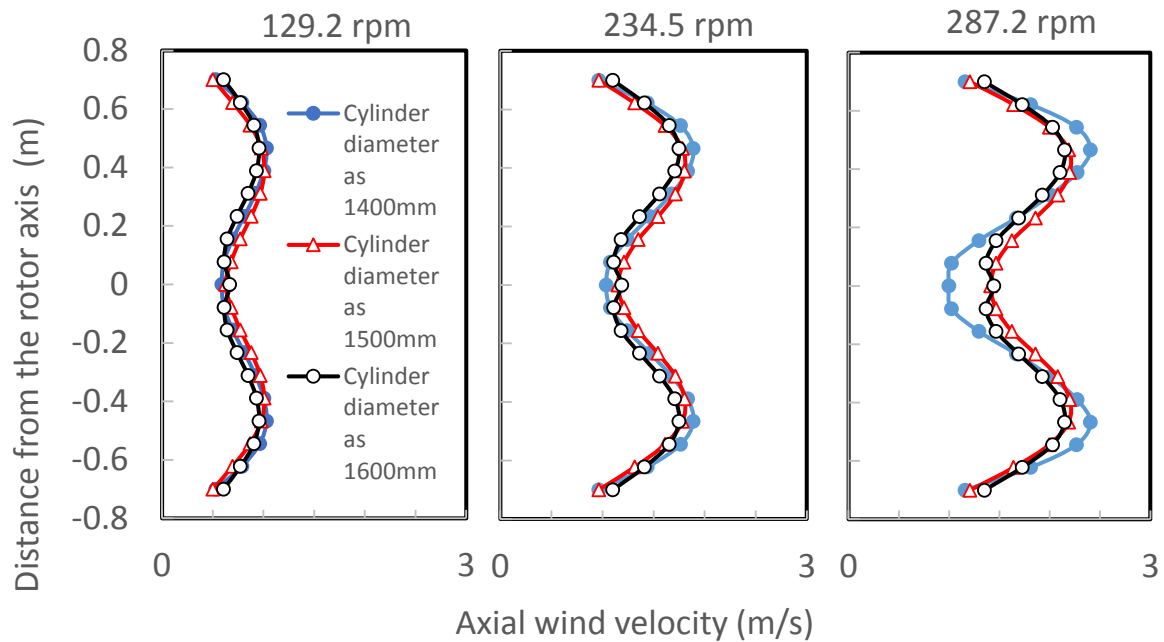


Figure 4.10- Effect of diameter of the test cylinder

Effect of the Size of the Test Chamber

In the different test standards available in different countries, the size of the test chamber that the efficiency of the ceiling fan is evaluated is specified different from an another. Therefore, the effect of the size of the test chamber on the measured parameters were also evaluated at the three RPM values specified above.

The height of the test chamber is almost identical on all standards; 3000mm, except a slight deviation in US ANSI standard which is 3352 mm. Since the average room height is ~ 3000 mm (10 ft) in many standard rooms, in this study, the room height was kept as constant 3000 mm while changing the width and the length. The obtained data are illustrated in Figure 4.11 below.

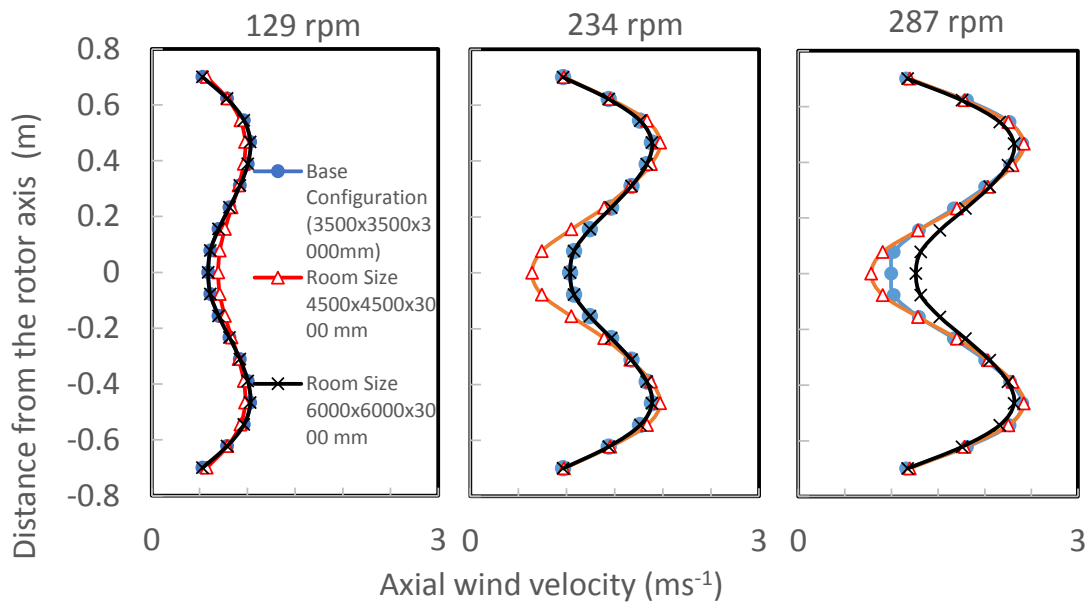


Figure 4.11 - Effect of the size of the test chamber

4.2.2 Case 2: Analysis of The Flow Field Characteristics Around Rotating Ceiling Fan Blades

In this case, the effort was to analyse the flow physics around a rotating ceiling fan. The characteristics which can be utilised in the design of more efficient fan was prioritised in the analysis. Initially, a mesh sensitivity analysis was performed to select the most economical and accurate mesh, then results of that mesh was assessed against experimental data in order determine the accuracy of the CFD model.

Similar to the previous case, the same setup as the experimental case was simulated by CFD and results were obtained. The analysis was then performed by considering the iso surfaces and contours of these simulations, which is described in the next section.

Validation

For the validation of the CFD case, axial velocity along the radial distance of the fan and the flow rate was assessed. In order to obtain a specially averaged value for the axial velocity, results were obtained across 11 arbitrary lines spanning 120° and the average value was obtained. In order to

obtain temporal averaged value, specially averaged values were taken across 0.1s at 0.02 time intervals and average was attained.

Mesh Sensitivity Analysis

A sensitivity analysis was performed on the grid resolution in order to establish mesh independence. Three grids were analysed with different sizes and number of cells, as depicted in table 4.7 below. The variation of the output velocity along radial direction, averaged velocity and mass flow rate was analysed. It was seen that these parameters do not depend significantly on the grid size at the selected values, a slight spike was seen on the velocity values directly under the centre of the fan of the 9.5M and 14.4M meshes. Based on these data 9.5M mesh was selected for further calculations Considering the computational cost and the resolution of data output. This is illustrated in figures 4.12 and 4.13.

Mesh Size	Average Velocity	Mass Flow
7.6 M	1.69 ms ⁻¹	2.97 kgs ⁻¹
9.5 M	1.70 ms ⁻¹	2.92 kgs ⁻¹
14.9 M	1.78 ms ⁻¹	2.98 kgs ⁻¹

Table 4.6- Variation of output with mesh size

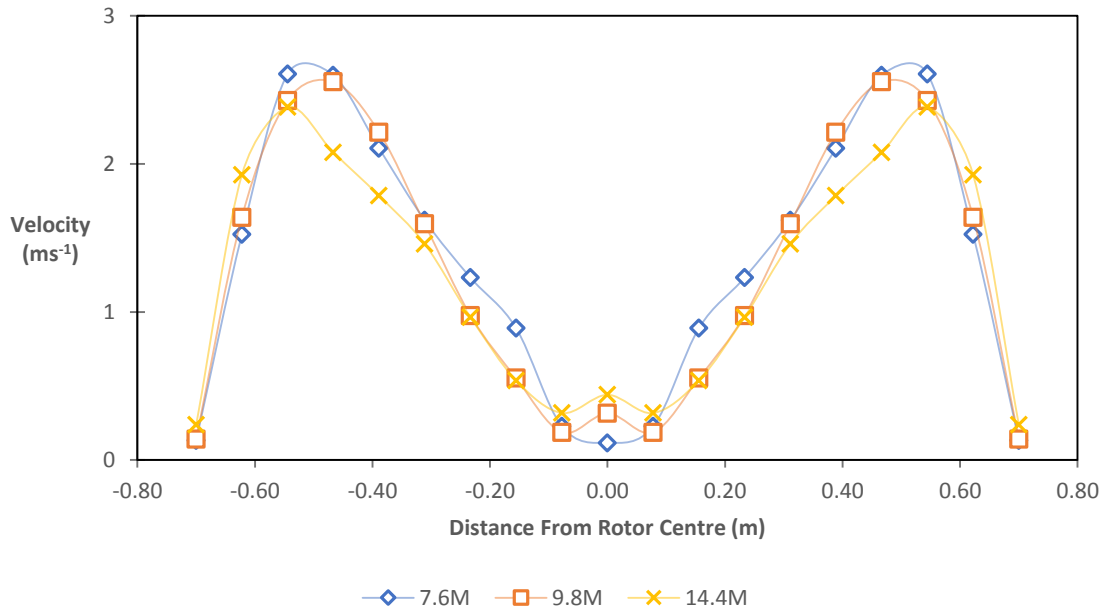


Figure 4.12 – Axial velocity variation

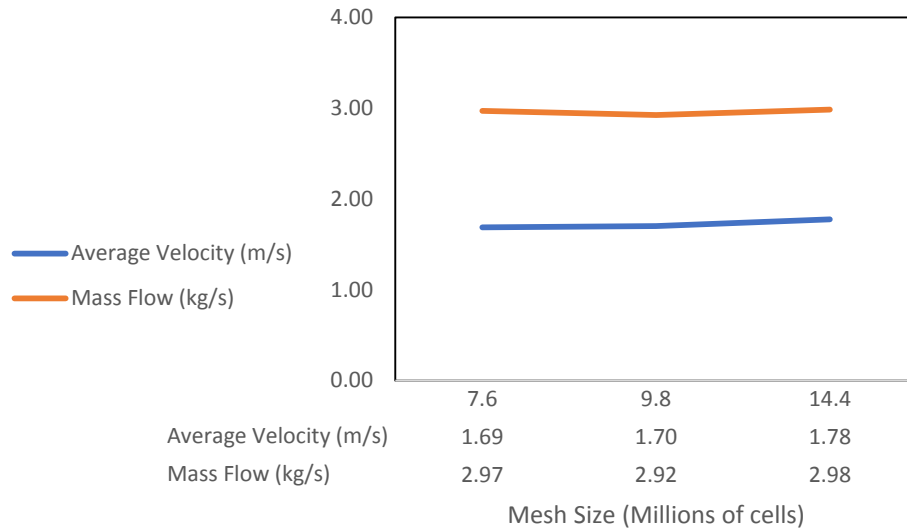


Figure 4.13 – Output value variation with mesh size

Validation against experimental data

Although the predicted results from the CFD simulation should be assessed against experimentally measured values in order to establish the accuracy of the generated model, direct comparison between the two cases is not feasible as the results from LES contain a lot more variation due to the resolution of eddies at a much lower time scale. Therefore, in order to normalize the data, the data over 6 seconds of simulation time was processed and the best fit polynomial of 5th degree was calculated. This was performed by importing the data to MATLAB. In order to normalize this set of data with the experimental data which was collected at 2 second intervals, the time averaging was done by considering data at 2 second intervals only. The result is shown in figure 4.14. By assessing this, it is in fact evident that the simulated data are in good agreement with the experimentally measured values, though a slight deviation is present in the maximum value. The error between the two is very low, the calculated NRMSD was 10%. Therefore, it can be concluded that LES initialised by a case of RNG KE can be used to predict the flow around a rotating fan blade with reasonable accuracy.

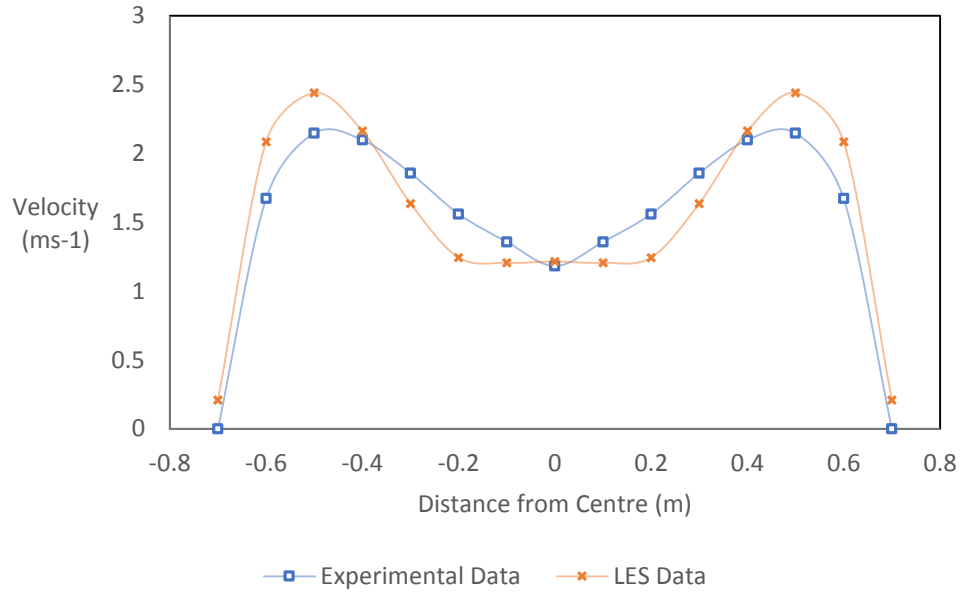


Figure 4.14 – Computational results for the selected RPM

Simulated Data

The simulation was carried out at the selected mesh configuration for a time period of 6.4S, which amounts closely to 25 revolutions of the fan. Although in previous work, LES analysis of rotating fans have been performed at simulation times as low as two revolutions of the rotor [63].

Axial velocity collected at 7 points at 0.1m intervals in radial direction just below test cylinder, in 5 lines at 30° to each other are averaged in order to obtain a spatially averaged solution and is given in the figure below.

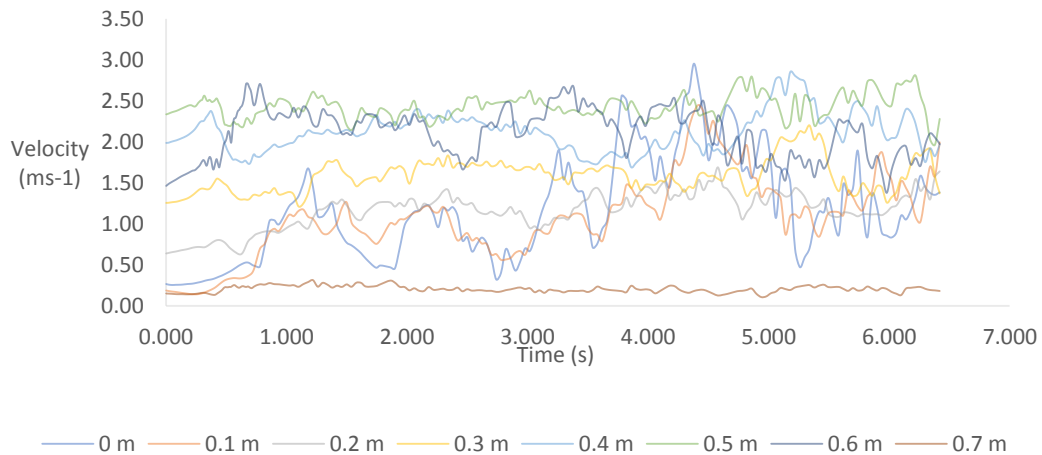


Figure 4.15 – Area averaged results of 7 points at 0.1m intervals in radial direction just below the cylinder

5. DISCUSSION

5.1 Experimental Data

The flow parameters under different RPM values corresponding to regulator settings of the employed ceiling fan is calculated for the experimental case and is given in the table below.

Regulator Setting	RPM	Maximum air velocity	Power Factor	Input Power (W)	Corrected Power	Mean Flow Delivery (Q)
1	129.2	1.2	0.48	16.7	16.9	94.1
2	180.5	1.7	0.61	27.7	28.0	133.2
3	234.5	2.1	0.76	41.6	42.2	171.2
4	258.3	2.4	0.85	49.6	50.2	189.0
5	287.2	2.5	0.98	60.9	61.7	203.7

Table 5.1 – Flow parameters at different RPMs

It can be observed that as expected the regulator setting one gave the lowest axial velocities and the regulator setting 5 gave the highest axial velocity values. Further, it is evident that the percentage increase of the velocities are decreased when the regulator setting is increased from 1 to 5, as shown in figure 5.1 (b). With the increase of average velocity with the regulator setting, the flow rate is increased as well.

The flow rate is the mass flow generated by the fan in axial direction. Flow coefficient reflects the performance of a ceiling fan in transferring the tangential velocity of the fan blade to the axial velocity component in air. The axial velocity is the effective component that provides thermal comfort. The tangential velocity component of the air is considered as a wastage. The Service Value reflects the ratio between the mass flow generated per the electrical power input into the fan blades.

The flow coefficient does not have a significant impact with different RPM values in this test case. The highest flow coefficient is seen at regulator setting 3 (234.5 RPM) and the service value decreases gradually from regulator setting 1 (129.2 RPM) to regulator setting 5 (287.2 RPM). This is due to the fact more power is required to rotate the fan at higher RPM values, which in turn cutback the effect caused by the increase of flow rate.

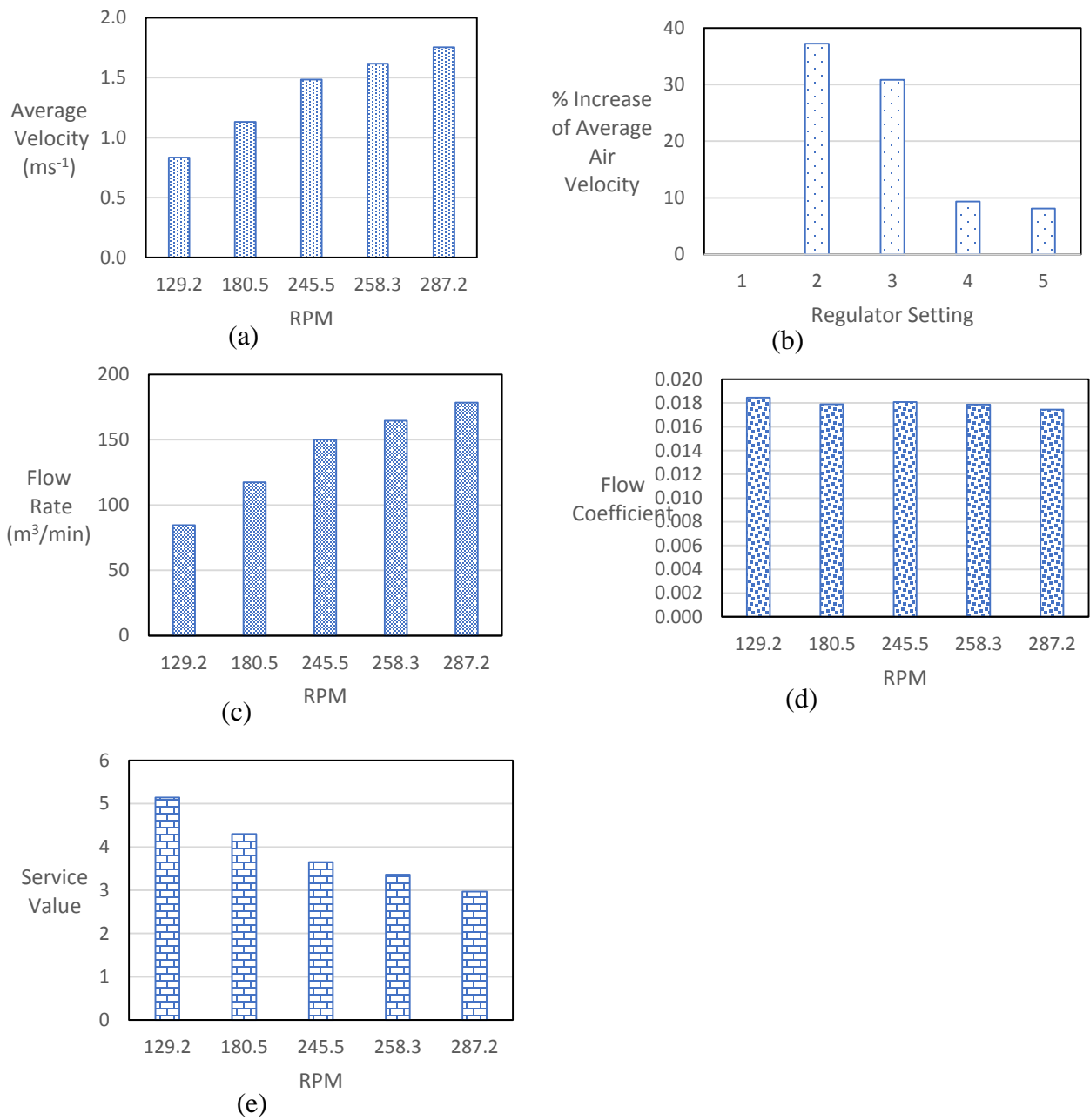


Figure 5.1 – Measured parameters at different regulator settings
 (a) – Variation of average air velocity with regulator setting
 (b) – Percentage increase of average air velocity with regulator setting
 (c) - Variation of flow rate with regulator setting
 (d) - Variation of flow coefficient with regulator setting
 (e) - Variation of service value with regulator setting

The energy rating is calculated for this fan according to the method described in section 3.1.6. The performance grade (PG) for this fan was calculated as 57.39, giving this fan an energy rating of three stars, as per the SLS standard 1600:2011. The key for energy ratings is given in table 5.2. The same energy rating was calculated by CFD methods and is given in table 5.5 in comparison with the experimental values.

Performance Grading (PG)	Star Rating
$PG \geq 85$	Five stars *****
$70 \leq PG < 85$	Four stars ****
$55 \leq PG < 70$	Three stars ***
$40 \leq PG < 55$	Two stars **
$30 \leq PG < 40$	One star *

Table 5.2 – Key for energy rating as per SLS 1600:2011

It is to be noted that in the calculations using experimental data, it is the standard practice at the Sri Lanka Standards Institute (SLSI) to substitute the measured axial velocity of the sensor directly below the barrel with zero, in order to reflect the boundary layer effect caused by the barrel wall, though with the measured experimental values, it is not zero. This can be due to various reasons such as the fact that there can be a slight misalignment between the cylinder wall and the sensor, and as a slight distance between the cylinder and the sensor in the vertical plane is present. This factor is validated with CFD results, which indicate that the axial velocity directly below the cylinder wall is indeed zero or very close to zero as depicted in Figures 4.5 and 4.6. To reflect this, the same procedure is practiced, so the axial velocity of the sensor directly below the cylinder wall is substituted with zero of experimental data, in these calculations.

5.2 Case 1: Analysis of the effect of ceiling fan test chamber geometry on the performance measurement of ceiling fans

Upon comparison of the calculated axial velocity values at a height of 1m below the plane of rotation of the fan in test cases with different test cylinder geometries, depicted in Figures 4.8 through 4.11, it is evident that the test cylinder geometry does not have a considerable effect on the axial velocity component. This is summarised in Figure 5.2. It is noted that the velocity at the extreme points in the case of barrel height at 914mm is deviating from the rest of the data set, and this is due to the fact that the plane of measurement, which is at 1m below the rotation of the fan is closer to the lower edge of the test cylinder, therefore the effect of the boundary layer of the cylinder wall is influencing this reading. In other cases, there is a significant distance between bottom edge of the barrel and the measurement plane, which in turn reduces the effect if this boundary layer on that point.

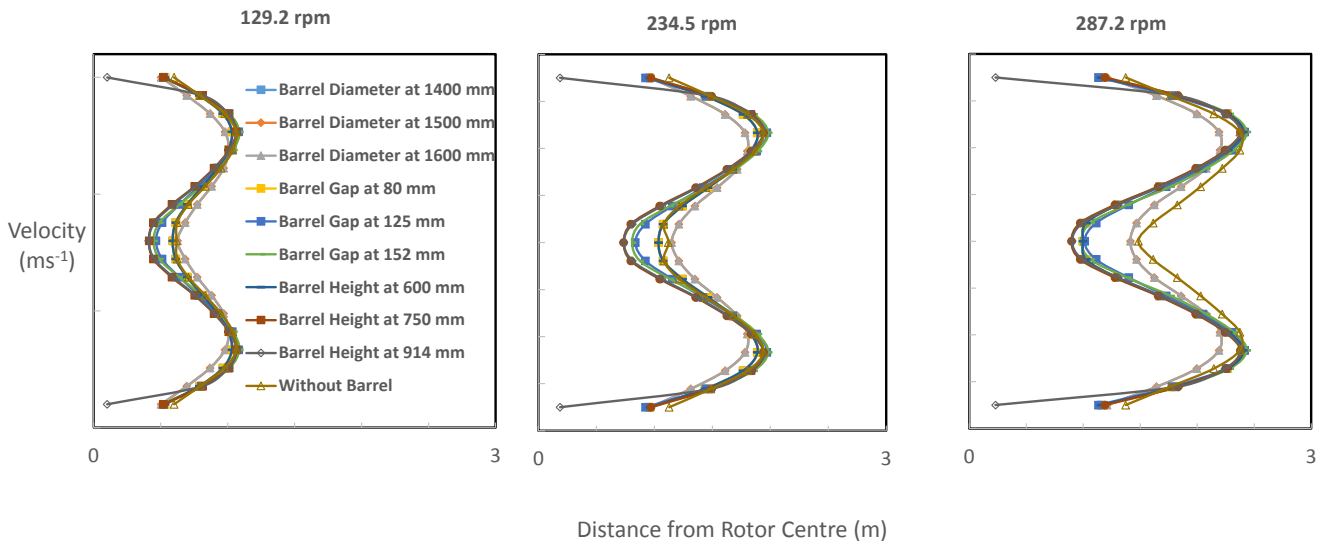


Figure 5.2 – Comparison of axial velocities 1m below the plane of rotation of fan

By this, it is evident that having a test cylinder does not have an appreciable effect on the measured axial velocity values. In order to further investigate this, a case with and without a test cylinder as compared at three RPM values, depicted in figure 5.3. By analysing this, it is confirmed that having a test cylinder has no considerable effect on the measured axial velocity of performance analysis of ceiling fans.

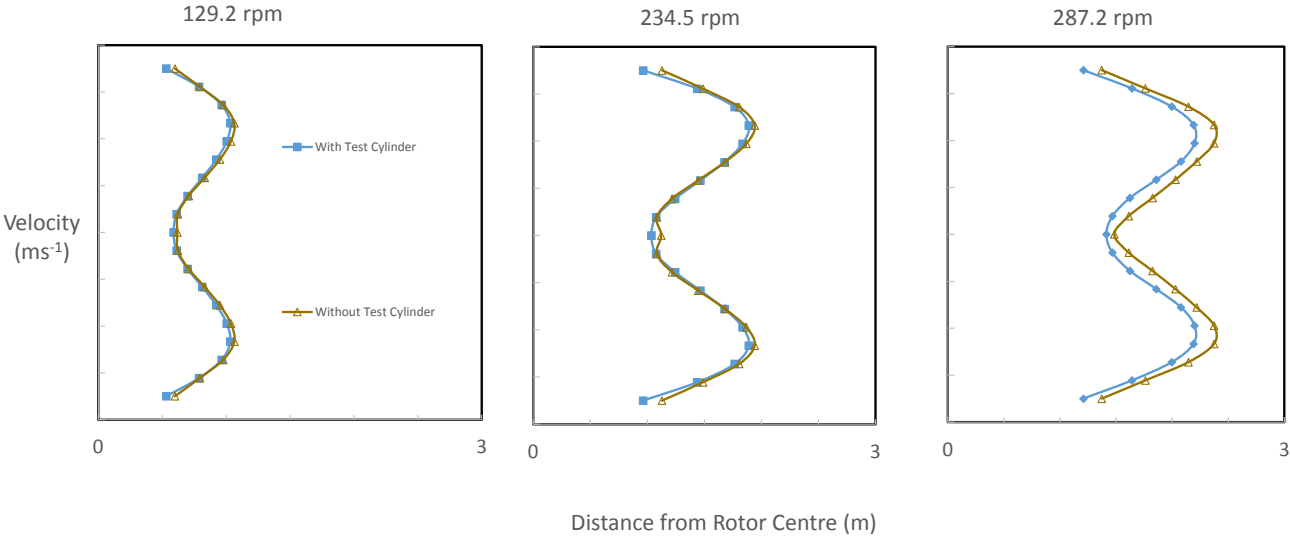


Figure 5.3 – Comparison of axial velocities at a height of 1m below the plane of rotation of the fan between a case with and without a test cylinder

In order to quantify the deviation in each case, the velocity values are compared with a case that does not contain a barrel, and NRMSD were calculated. The calculated NRMSDs are presented in table 5.3.

Case	NRMSD (%)		
	129.2 RPM	234.5 RPM	287.2 RPM
Without Cylinder	Reference Case	Reference Case	Reference Case
Cylinder Diameter at 1400 mm	1.91	2.26	7.50
Cylinder Diameter at 1500 mm	4.43	4.90	4.97
Cylinder Diameter at 1600 mm	6.65	5.34	9.08
Cylinder Gap at 80 mm	1.91	2.26	7.50
Cylinder Gap at 125 mm	3.69	3.49	6.57
Cylinder Gap at 152 mm	3.92	3.65	6.57
Cylinder Height at 600 mm	1.91	2.26	7.50
Cylinder Height at 750 mm	4.99	4.52	7.73
Cylinder Height at 914 mm	6.08	6.09	7.35

Table 5.3 – NRMSD w.r.t. a case without test cylinder

It is evident that at higher the deviation is higher in higher RPM values. This can be due to the effect of turbulence at high velocities. But in other RPM values, it is evident that the deviation is quite low and the effect of the test cylinder is minimum. The maximum deviation is seen in the case which has the cylinder of diameter of 1600mm which amounts to approximately 9%. The minimum deviation is present in the cases with a cylinder with 1400mm diameter, 600mm cylinder height and a gap of 80mm between the cylinder and the plane of rotation of the fan, which corresponds closely with SLS 1600:2011.

The lack of variation of the axial velocity values results in negligible change in energy rating calculated between the cases with different cylinder geometries. Whereas, if a considerable misalignment was present between the fan and the cylinder, it would have a negative effect on the measured axial velocities, leading to errors in performance grading ultimately leading to false energy ratings. The calculated service value and flow coefficient of the cases tested is presented in Figure 5.4. This is summarised in table 5.4.

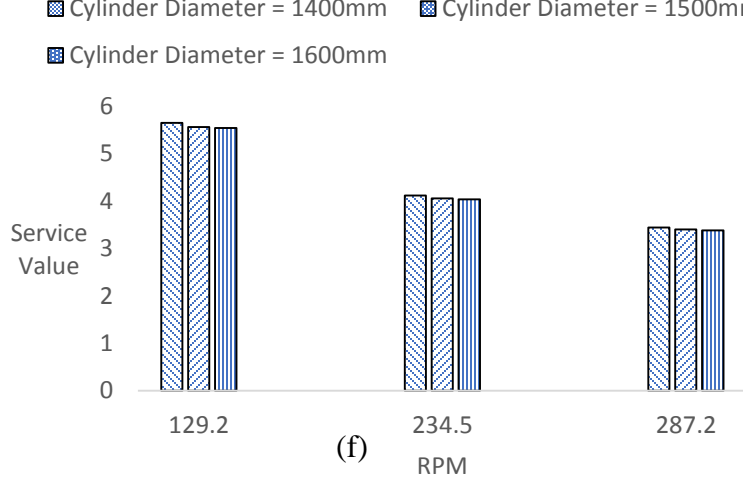
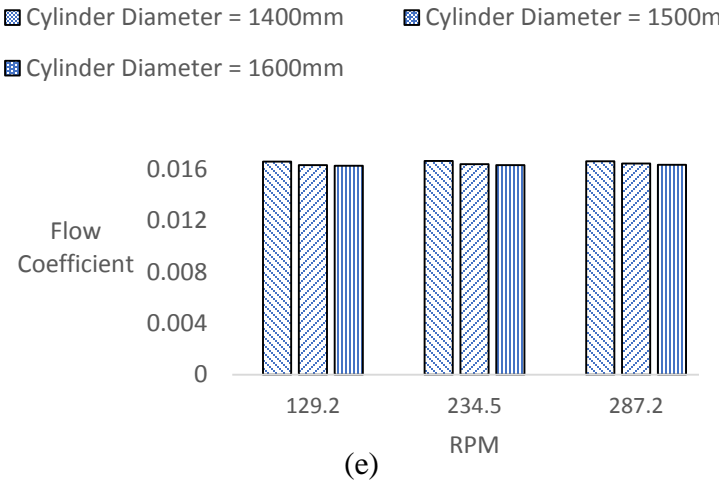
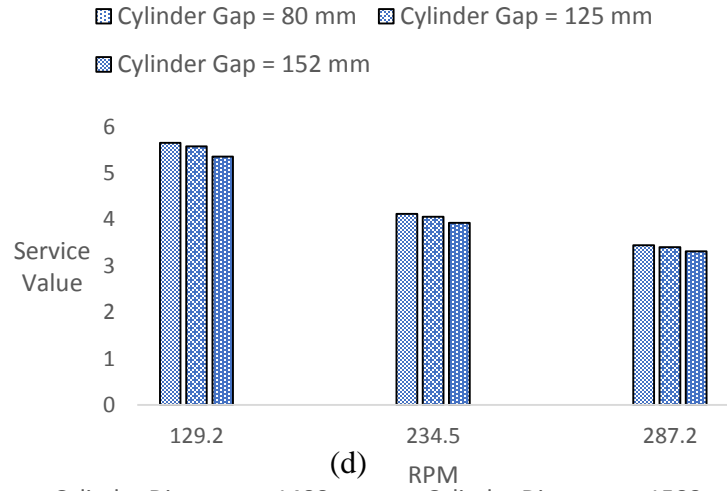
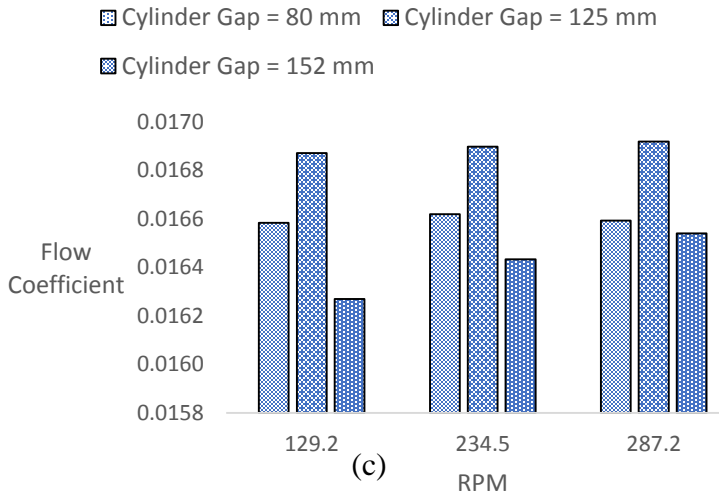
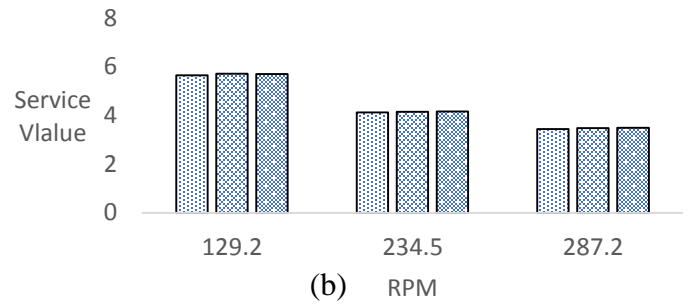
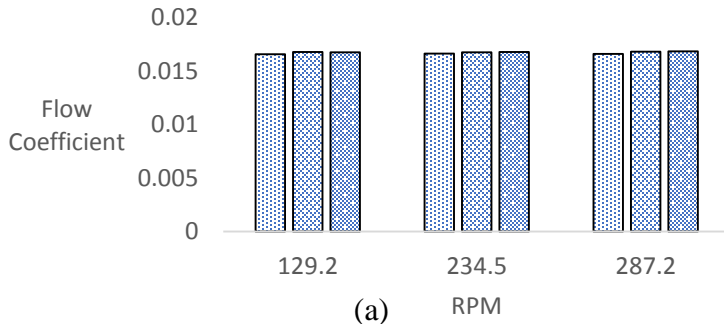


Figure 5.4 – Comparison of calculated values between tested cases

- (a) – Calculated flow coefficient in cases with different gaps between cylinder and fan
- (b) – Calculated service value in cases with different gaps between cylinder and fan
- (c) – Calculated flow coefficient in cases with cylinders with different diameters
- (d) – Calculated service value in cases with cylinders with different diameters
- (e) – Calculated flow coefficient in cases with cylinders with different heights
- (f) – Calculated service value in cases with cylinders with different heights

	129.2 RPM		234.5 RPM		287.2 RPM	
	Flow Coefficient	Service Value	Flow Coefficient	Service Value	Flow Coefficient	Service Value
Without Cylinder	0.017	5.948	0.017	4.287	0.017	3.600
Cylinder Gap = 80 mm	0.017	5.655	0.017	4.120	0.017	3.441
Cylinder Gap = 125 mm	0.017	5.719	0.017	4.154	0.017	3.484
Cylinder Gap = 152 mm	0.017	5.709	0.017	4.163	0.017	3.491
Cylinder Height = 600 mm	0.017	5.655	0.017	4.120	0.017	3.441
Cylinder Height = 750 mm	0.016	5.563	0.016	4.061	0.016	3.405
Cylinder Height = 914 mm	0.016	5.542	0.016	4.041	0.016	3.385
Cylinder Diameter = 1400mm	0.017	5.655	0.017	4.120	0.017	3.441
Cylinder Diameter = 1500mm	0.017	5.575	0.017	4.059	0.017	3.400
Cylinder Diameter = 1600mm	0.016	5.353	0.016	3.931	0.017	3.310

Table 5.4 – Summary of calculated service value and flow coefficient in cases with different cylinder geometries

Upon calculation of these parameters, it is evident that a considerable effect on the service value nor the flow coefficient measured ultimately leading to little or no impact on the efficiency measurement of ceiling fans. Therefore, energy star rating is calculated according to the method specified in 3.1.6 above for the case with and without a test cylinder and is compared with experimentally calculated energy rating. For the case with cylinder, the geometry is selected as per SLS standard 1600:2011. This is presented in table 5.5 below.

Case	Performance Grade (PG)	Energy Rating
Experimental	57.39	Three Stars (***)
Simulation With Test Cylinder	59.41	Three Stars (***)
Simulation Without Test Cylinder	60.16	Three Stars (***)

Table 5.5 – Calculated energy rating of different cases

Therefore, it is evident from this calculation that having a test cylinder does not have a significant impact on the energy rating. The percentage deviation of performance grading without the test cylinder is 1.2%. Installing a cylinder as per the standards and aligning it correctly with the test fan requires lot of effort and the fabrication of the cylinder amounts to a considerable portion of cost of the test setup. Further having a misaligned cylinder can lead to far inaccurate results. Therefore, considering the very low impact having a test cylinder have on the calculated performance grade, it can be said that the test cylinder can be neglected from the test setup for testing ceiling fan performance. This is aligned with the decision by United States Department of Energy (DOE) decision to remove the test cylinder from ceiling fan test standard from January, 2017 [16].

The size of the room does not have a significant impact on the velocities measured for the performance analysis of the fans, as long as sufficient gap is maintained between the fan and the ceiling, but does have an impact of the overall flow in the room [64] [41]. This is further evident from the calculated service value and flow coefficient parameters.

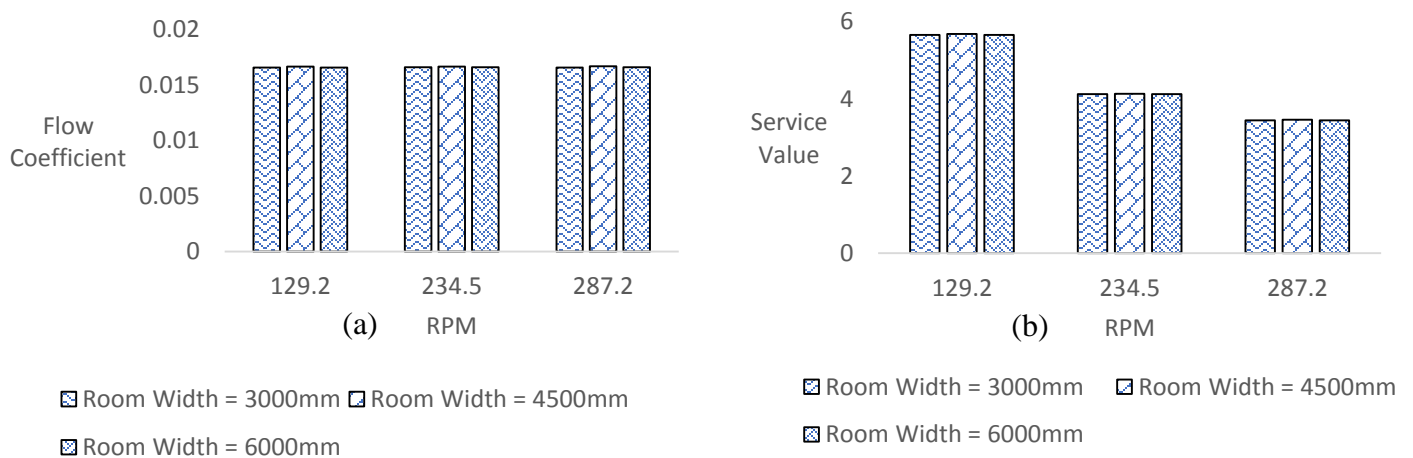


Figure 5.5 – Comparison of calculated values between cases of different room sizes
 (a) - Calculated service value in cases with different room sizes
 (b) - Calculated flow coefficient in cases with different room sizes

5.3 Case 2: Analysis of the Flow Field Characteristics Around Rotating Ceiling Fan Blades

Axial velocities at different points throughout the LES simulation differs significantly with time as this method models the effects of all the eddies that lead to turbulence in the inertial subrange. Thereby, as stated previously in the section “validation with experimental data”, the data is required to be normalized to obtain a meaningful understanding. This clearly seen when the axial velocity of points along the radii of the fan are plotted against time of simulation. Figure 5.7 shows velocity variation with time of 8 points at 100mm apart from each other at 5 lines along radius of the fan. Lines are separated from each other by 30° . The chaotic distribution of the flow can clearly be identified from this. The generation of vortices can be verified by analyzing the iso surfaces of q criterion and through vorticity and is depicted in this chapter below.

A clearer understanding can be obtained by calculating the spatially averaged solution along the radii of the fan for 120° angle, as depicted in figure 5.6 below.

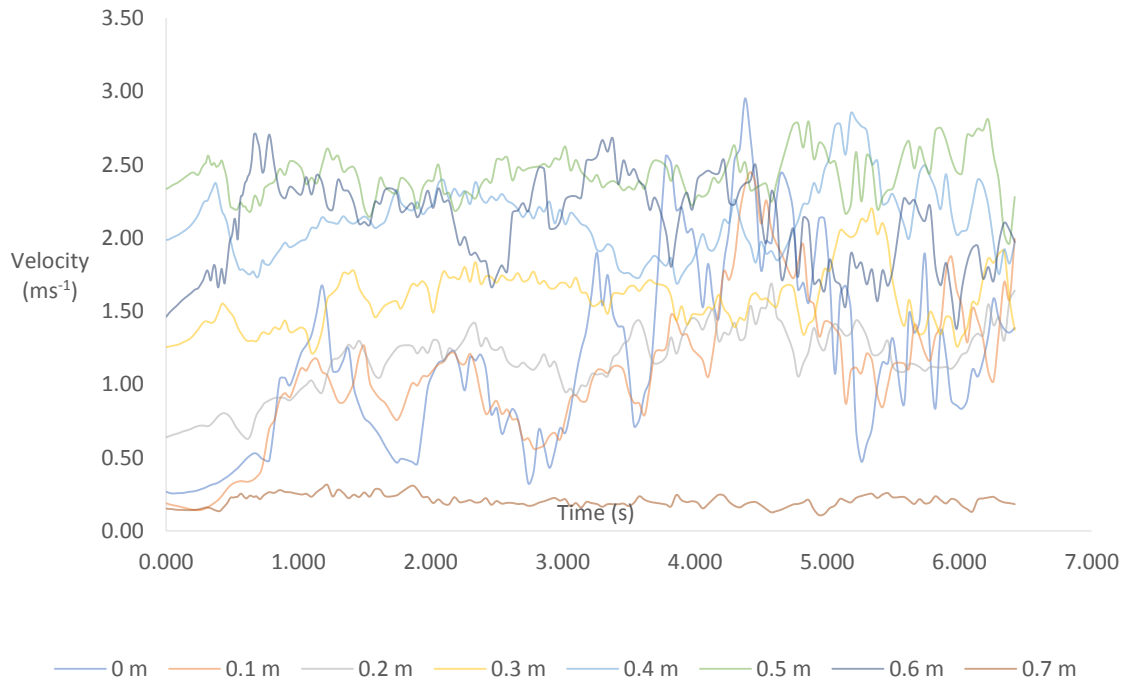


Figure 5.6 – Spatially averaged axial velocity variation of 120° angle along radii of the ceiling fan with time

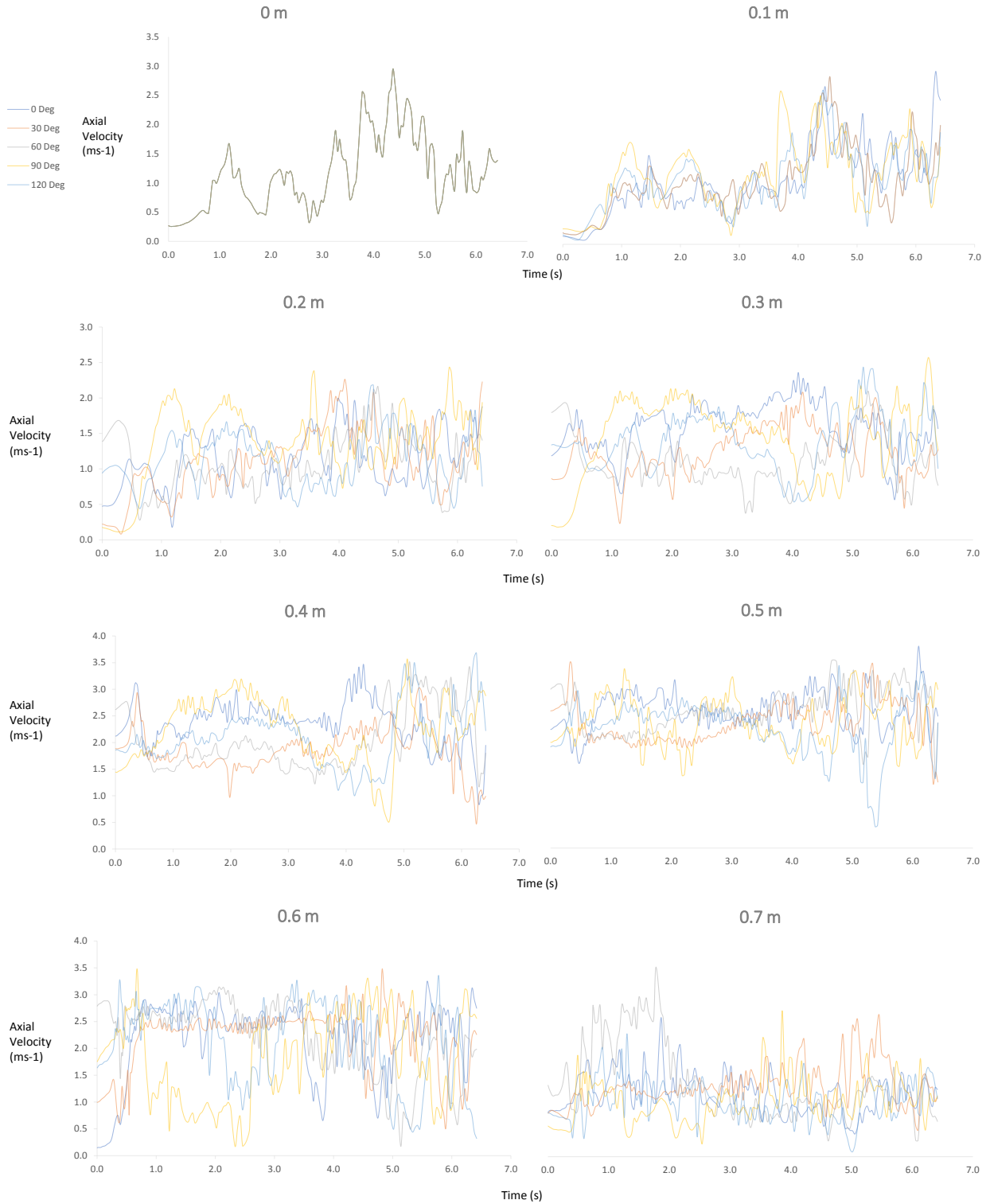


Figure 5.7 – Variation of axial velocity at 8 points at 100mm intervals along the radii of the ceiling fan with time in 5 lines along the radii of the fan at 30° intervals

Figure 5.8 shows instantaneous velocity vectors at one line at different flow times in comparison with experimental data.

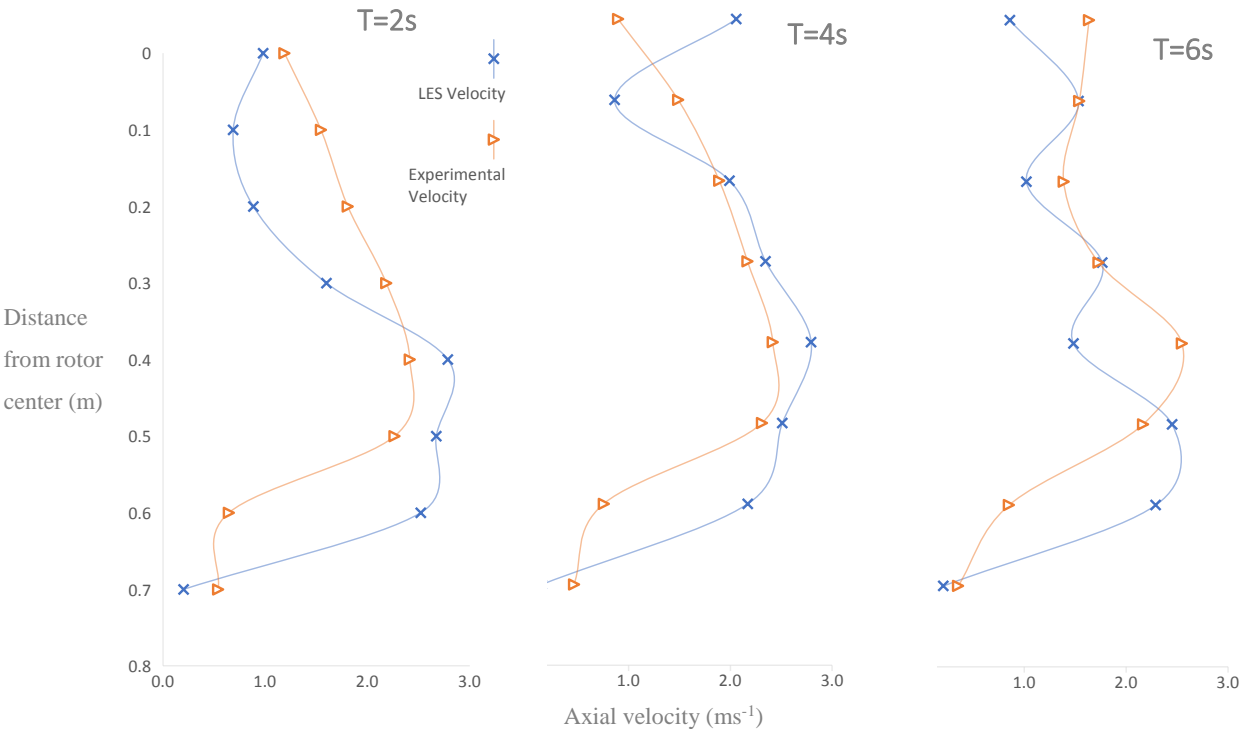


Figure 5.8 – Instantaneous velocity vectors at 8 equally spaced points on one line at different flow times in comparison with experimental data.

The formation of vortical structures in the air volume can be visualized when contour of vorticity magnitude is plotted. Initially, vortical structures are not visualised due to the RANS initialisation. These starts appearing at around 0.1 seconds of flow simulation originating from the tip of the blade as a result of vortex shredding phenomenon. With the flow time, the vortices get pushed down with the flow as new vortical structures are formed at the blade tip. As these vortical structures move further downward, more vortices are formed due to the action of these and the number of vortices keep growing with flow time, resulting the flow to become turbulent with the flow time. This is illustrated in figure 5.9 below.

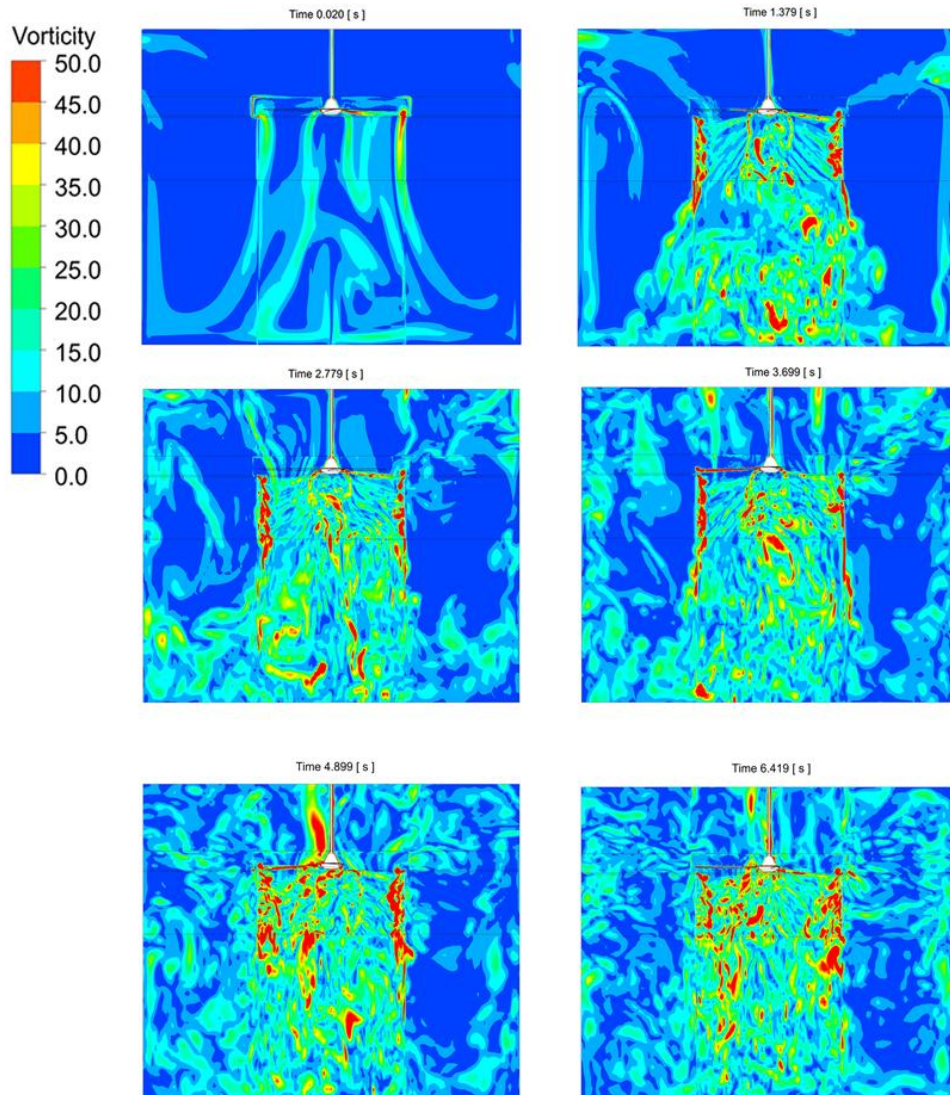


Figure 5.9 – Formation of vortical structures

The turbulent nature of the flow is further revealed upon analysing of the vertical contours of the velocity vector as shown in figure 5.10 below. Turbulent nature of the flow start from the rotating fan and it eventually moves downwards. As it approaches the floor of the room, the flow spreads out towards the walls of the room and it moves upwards, in reverse direction at it reaches the top side of the fan again completing the rotational cycle of the flow. This confirms the results of previous researches which state that the flow moves upwards along the walls of the room and reaches the suction side of the ceiling fan again [32] [2].

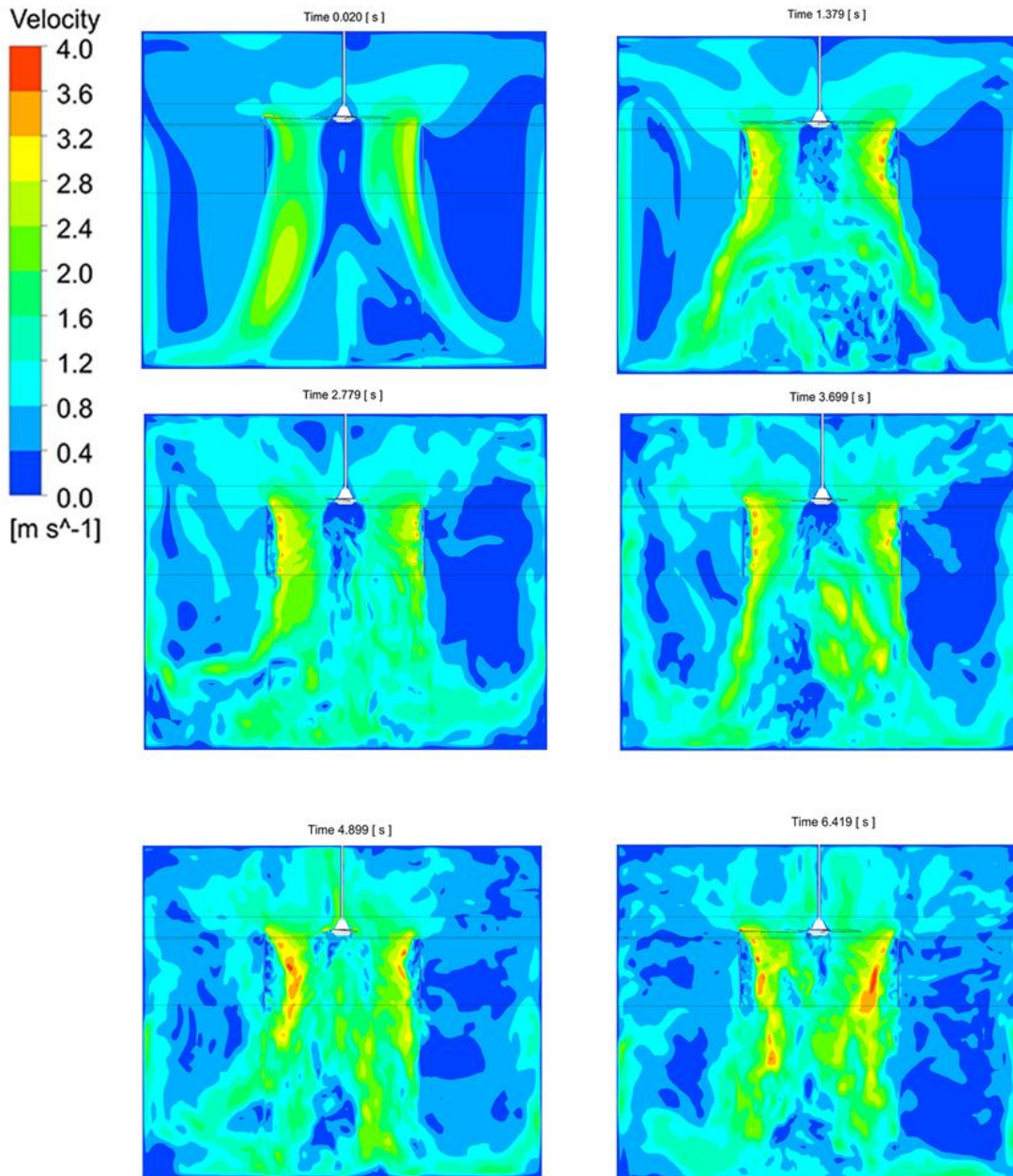


Figure 5.10 – Vertical contour of velocity through centre of rotation of fan

The formation of vortical structures from the blade tip is further evident by analysing the ISO surface of Q criterion. Figure 5.11 shows the iso surface of Q criterion at $Q = 3000 \text{ s}^{-2}$ colored by velocity magnitude.

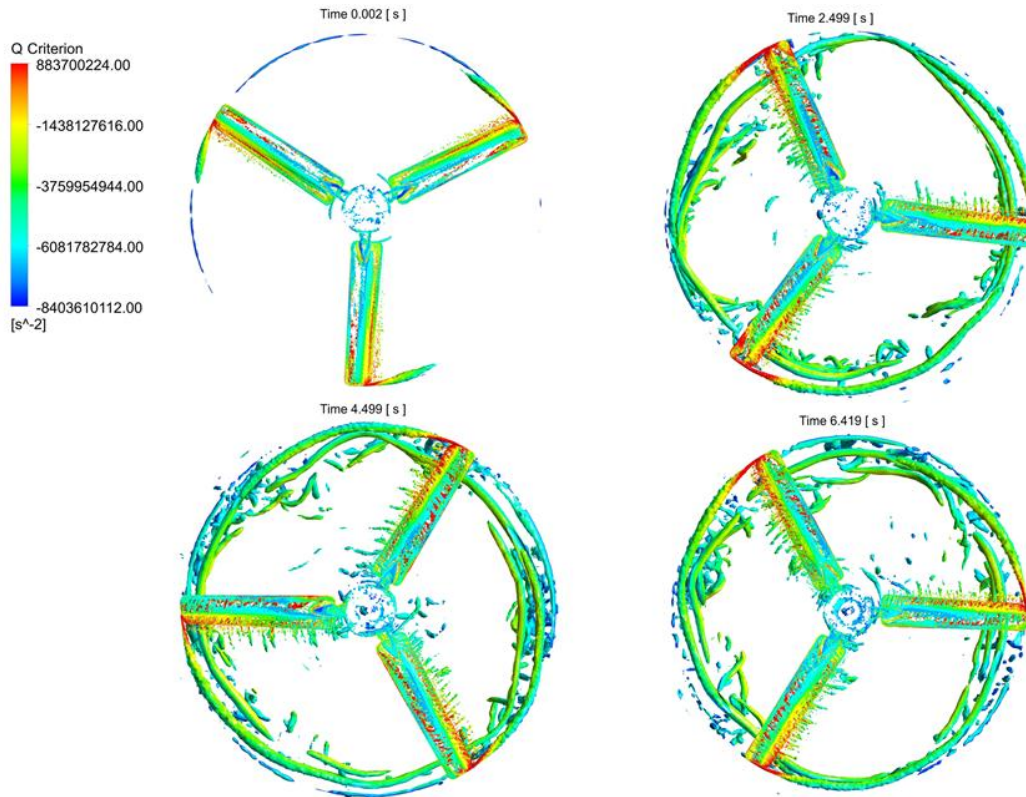


Figure 5.11 – Iso surface of $Q=3000 \text{ s}^{-2}$ colored by velocity magnitude

This contour shows that the flow transition from laminar to turbulent occurs at the mid chord section, starting from the deflected section of the blade. Further the creation of two major vortical structures is seen arising from the tip and the root of the blade, in this contour. The transition to turbulent flow can be further verified by the instantaneous contours of velocity plotted on the iso surface of vortex core region (at vorticity = 250 s^{-1}). The formation of the vortical structures behind the deflection line of the blade is clearly visualised by this. The formation of the vortical structures starts at about 0.2 chord length from trailing edge at the root of the blade and increases up to about 0.4 chord length at the tip of the blade, as seen in figure 5.12.

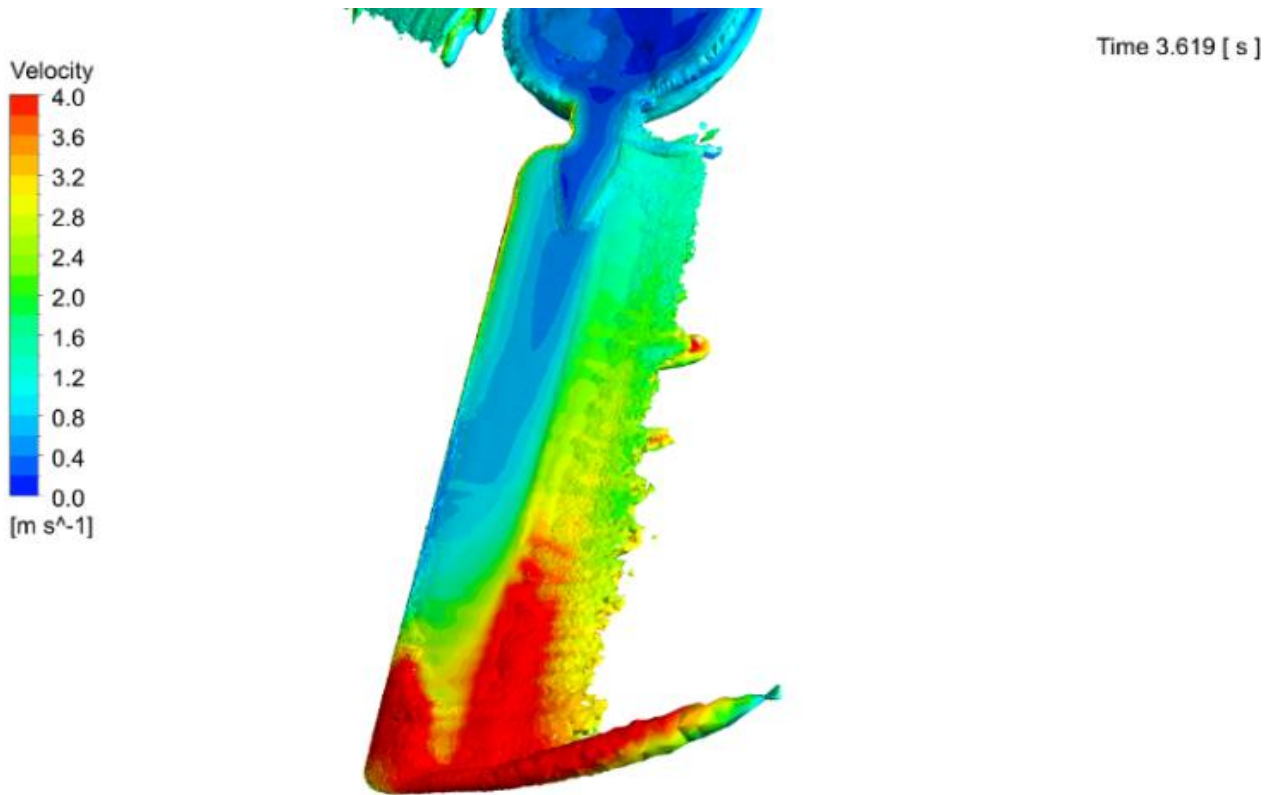


Figure 5.12 – Iso surface of vortex core region at Vorticity = 250 s^{-1} colored by velocity

This formation of numerous circulations is supported by Pandtl lifting line theorem, which states that a local circulation will arise with change in lift in the spanwise direction [65]. In this sense, the formation of the larger circulating flow at the tip of the blade can be said to be occurring due to the higher change in lift at the blade tip. At the chordwise point at which these circulating structures starts appearing, the flow can be said to be separated.

The formation of the tip vortex is clearly seen by vector plot in the mid-section of the fan blade. The formed vortex then travels downstream with the flow, to the opposite direction of the rotation of the fan blade, while moving downwards with the downwash, as seen by the iso surface of Q criterion, at $Q = 10000 \text{ s}^{-2}$.

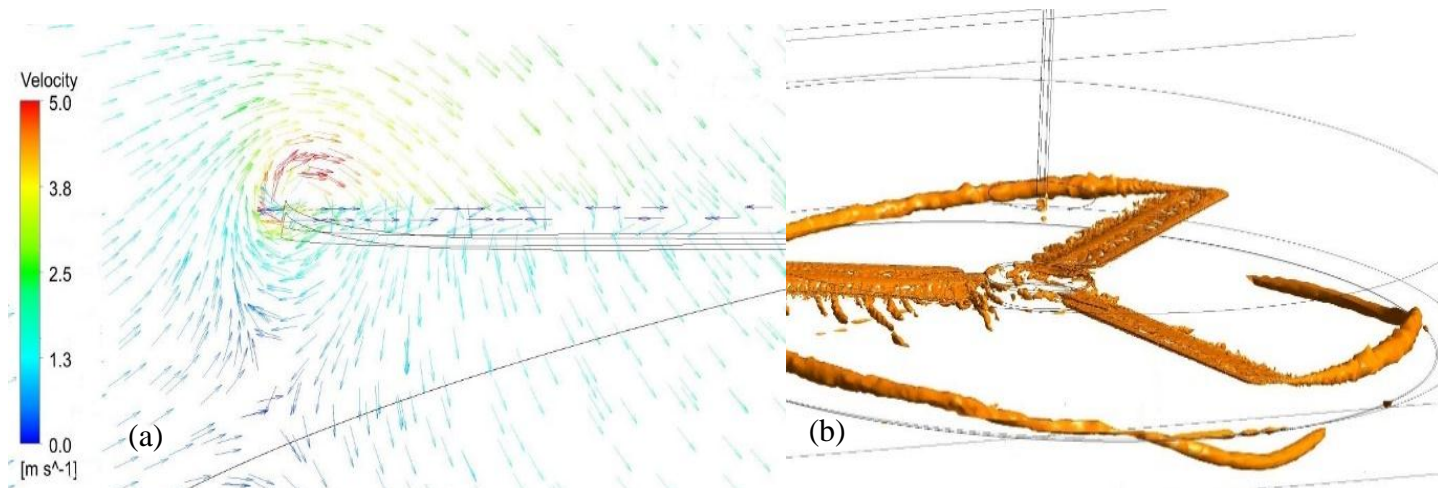


Figure 5.13 – Formation of vortical structures
 (a) – Vector plot of velocity colored by velocity at mid-section of the fan blade
 (b) - Iso surface of Q criterion, at $Q = 10000 \text{ s}^{-2}$

This vortex gradually increases in size as it moves downstream. This is visualised by the instantaneous contours of vorticity plotted at vertical planes parallel to the blade at $x= 12\text{mm}$, 24mm and 36mm respectively from the mid point of the fan blade.

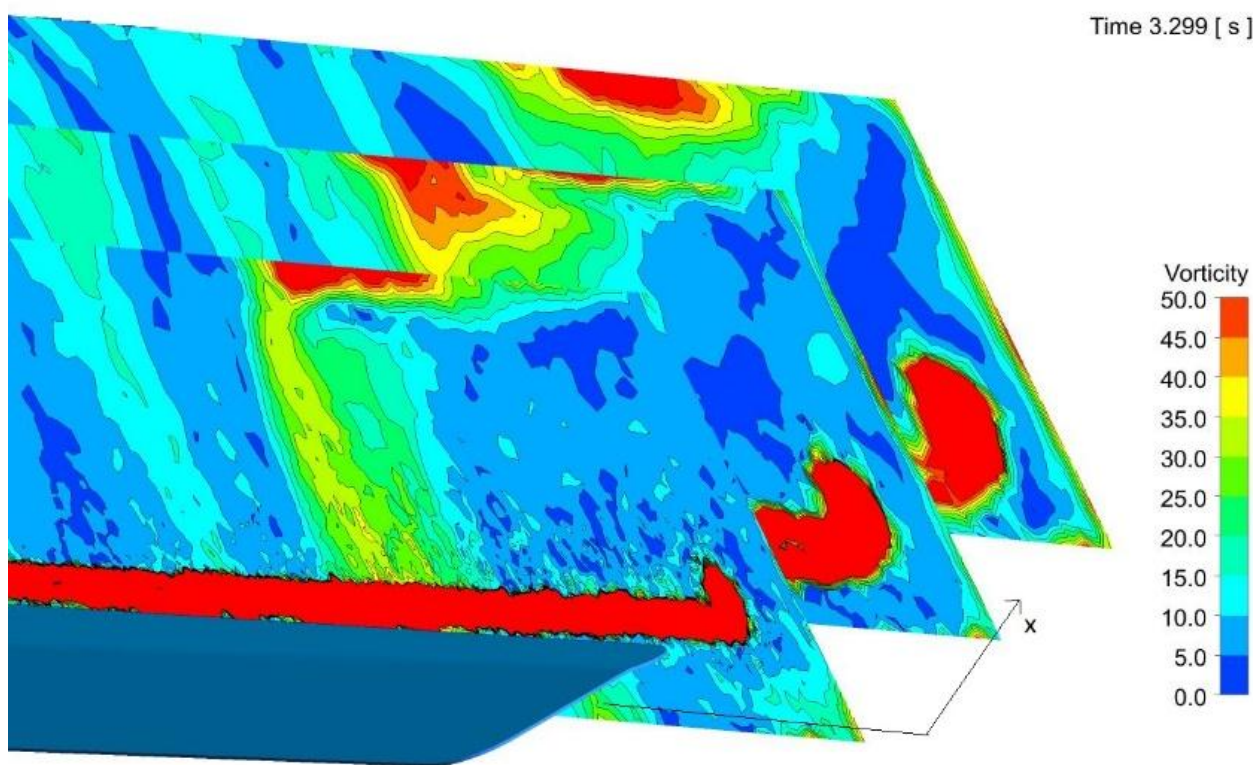


Figure 5.14 – Instantaneous contours of vorticity at vertical planes of $x=12\text{mm}$, 24mm and 36mm at a flow time of 3.299s

The separation point of the flow can be further realised by the contour of vorticity plotted on the bottom surface of the fan blade.

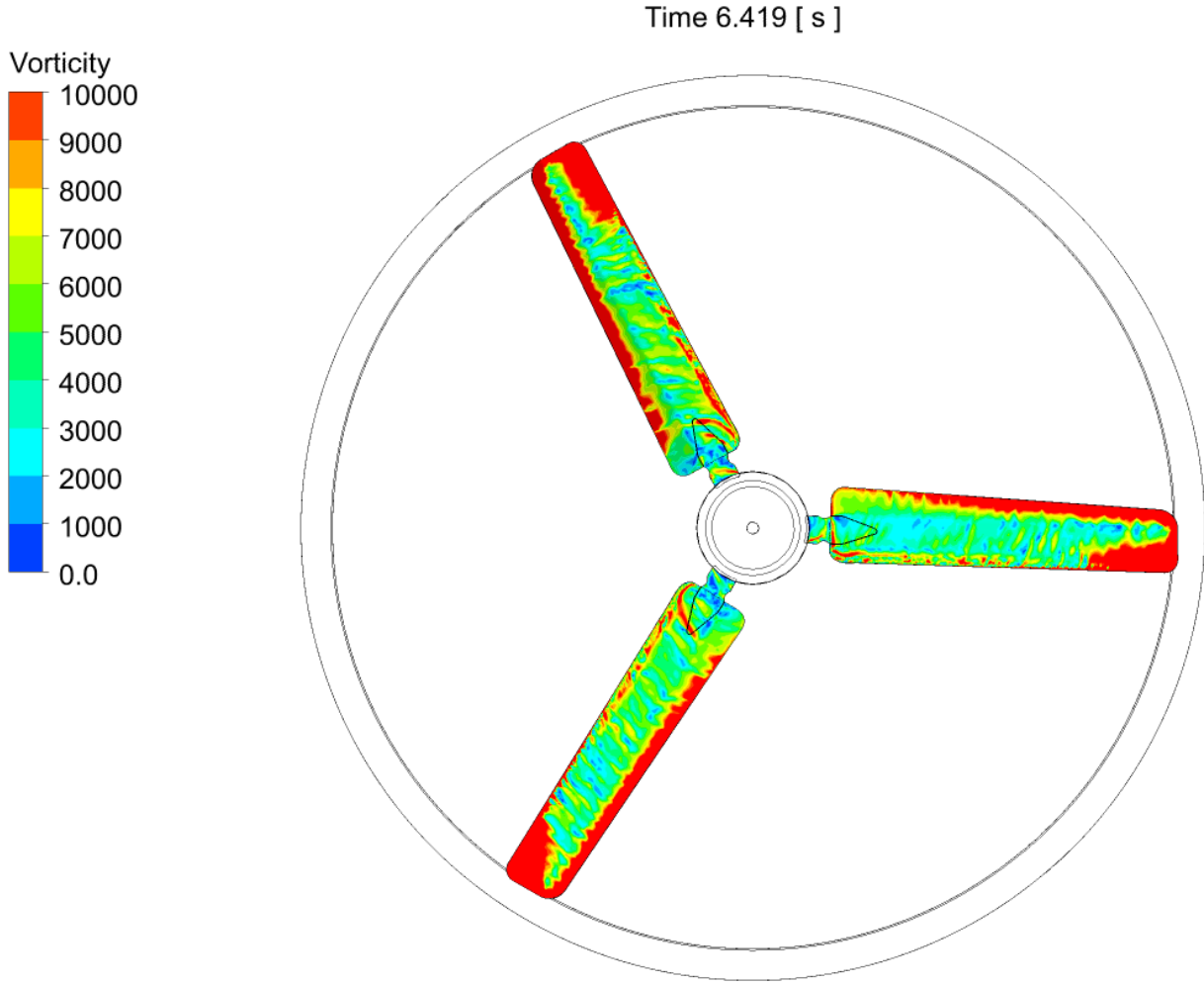


Figure 5.15 – Vorticity contour on the bottom surface of the blade

It is seen that the flow separation mainly occurs on the trailing edge of the fan blade. Further it is seen that the area of separation gradually increases in size when moving from root to tip, as mentioned previously. A larger localized area of separation is seen at the tip of the blade. This is due to the tip vortices as shown in figure 5.13 (a) previously.

From a contour of total pressure plotted on a vertical plane at the mid-chord section of the fan blade, it can be seen that the maximum pressure is present close to the tip of the blade, resulting more downward flow velocity closer the blade tip. This is due to the fact that the tangential velocity in a rotating object is directly proportional to the distance from the centre of rotation, R , resulting in maximum axial velocity being closer to the tip of the blade.

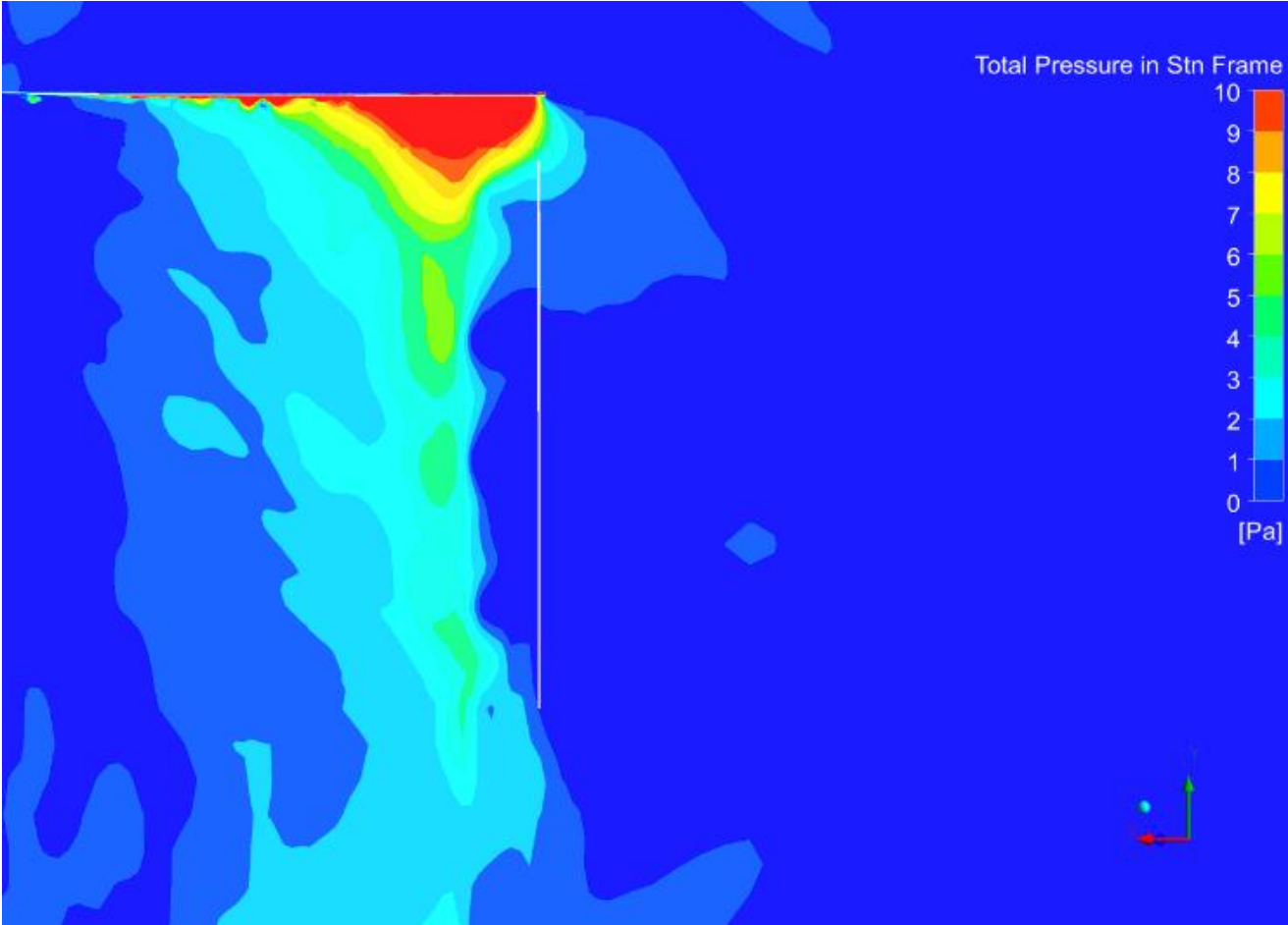


Figure 5.16 – Total pressure in the mid -chord section of the fan blade

6. CONCLUSION

The key aim of this research is to analyse the flow field around ceiling fans with thin blade profiles in standard test conditions and investigate on the effect of standard ceiling fan test setup geometry on the same via numerical methods. Thereby, investigating the effect of ceiling fan test chamber geometry on the performance evaluation of ceiling fans being one objective, a RANS simulation was carried out by modeling different ceiling fan test geometries. From these simulations, it is evident that having a test cylinder does not have a significant impact on calculation of the energy rating or the performance grade of a ceiling fan and can be neglected from the test setup. Further, it is seen that the size of the test chamber does not have a significant impact on measured values as long as sufficient and similar gap is maintained between the plane of rotation of the fan and the cylinder and the results are taken at similar heights from the plane of rotation of the fan.

Upon comparison of geometries from different test standards used in different countries across the world, is seen that the geometry specified in SLS standard 1600:2011 provides results with minimal influence by the test cylinder.

Further research is required to be conducted with more fan with different blade designs to arrive at a more general conclusion on the effect of the test chamber geometry on the performance evaluation of ceiling fans.

Also, from the Large Eddy Simulations, it is established that the flow generated from the ceiling fan spreads outwards as its moving downwards, gets deflected towards the walls of the room as it meets the floor of the room and travels upward against the downward flow along the walls towards the suction of the fan, completing a cycle. The air inside the room with a ceiling fan is highly turbulent, resulting in more thermal comfort for the occupants. A natural transition from laminar to turbulent flow can be seen close to the mid chord in the suction side of the fan blade.

From contours of iso surfaces of this simulation, it is seen that in the fan blades, two major vorticial structures are seemed to be formed, starting from the root and the tip of the blade. Between these two vortices, numerous amounts of small circulating structures can be seen as a result of lift differences at different point in the spanwise direction. Further, it is also seen that the maximum downward pressure is seen at approximately $0.8R$, in turn resulting in maximum velocity also being at the same location by plotting the contour of pressure in vertical direction.

These finding can be used as a basis for further research work for developing a more efficient fan blade design for ceiling fans.

7. REFERENCES

- [1] L. Rosario, S. H. Ho and M. M. Rahman, “Thermal Comfort Enhancement by Using a Ceiling Fan,” *Applied Thermal Engineering journal*, no. 29, pp. 1648-1656, 2008.
- [2] F. Babich, M. Cook, D. Loveday, R. Rawal and Y. Shukla, “Transient three-dimensional CFD modelling of ceiling fans,” *Building and Environment*, vol. 123, pp. 37-49, 2017.
- [3] F.H. Rohles, S.A.Konz and B.W.Jones, “Ceiling Fans Extenders of the Summer Comfort Envelope,” *ASHRAE Transactions*, vol. 89, no. Part 1, pp. 245-263, 1983.
- [4] J. Adnot, . L. Grignon-Massé and . P. Rivière , “Energy Consumption of European Residential Comfort Fans,” in *5th International Conference in Energy Efficiency in Domestic Appliances and Lighting*, Florence, 2009.
- [5] S. de la Rue du Can, . V. Letschert, M. McNeil, N. Zhou and J. Sathaye , “Residential and Transport Energy Use in India: Past Trend and Future Outlook,” Ernest Orlando Lawrence Berkeley National Laboratory, California, 2009.
- [6] P. Biermayer, J. Busch, S. Hakim, I. Turiel, P. Pont and C. Stone, “Feasibility of an Appliance Energy Testing and Labeling Program for Sri Lanka,” Ernest Orlando Lawrence Berkeley National Laboratory, California, 2000.
- [7] Energy Star, “Energy Star Certified Ceiling Fans,” Environmental Protection Agency, 15 June 2018. [Online]. Available: https://www.energystar.gov/products/lighting_fans/ceiling_fans. [Accessed 18 July 2018].
- [8] Sri Lanka Standards Institution, “Sri Lanka Standard Energy Efficiency Rating For Electric Ceiling Fans With Regulators,” Sri Lanka Standards Institution, Colombo, 2011.
- [9] Bureau of Indian Standards, “Specification for Electric Ceiling Type Fans and Regulators,” Bureau of Indian Standards, New Delhi, 2004.

- [10] A. G. T. Sugathapala and P. Somarathne , “Performance Analysis of Pedestal Fans an Experimental Investigation,” in *ERU Research Symposium, University of Moratuwa*, Moratuwa, Sri Lanka, 2000.
- [11] A. G. T. Sugathapala , “Wall Effects on The Performance of Ceiling Fans: A Two-Dimensional Model,” in *ERU Research Symposium, University of Moratuwa*, Moratuwa, Sri Lanka, 2000.
- [12] N. Sathaye, A. Phadke, N. Shah and V. Letschert , “Potential Global Benefits of Improved Ceiling Fan Energy Efficiency,” Environmental Energy Technologies Division International Energy Studies Group Lawrence Berkeley National Laboratory, 2013.
- [13] T.M.I. Mahlia, H. Moradalizadeh, M.N.M. Zubir and T. Olofsson, “Theoretical and Experimental Investigation of Energy Efficiency Improvement of the Ceiling Fan by Using Aerodynamic Blade Profile,” *Journal of Energy & Environment* , vol. 3, no. 1, pp. 40-49, 2011.
- [14] N. Sathaye, A. Phadke, N. Shah and V. Letschert, “Potential Global Benefits of Improved Ceiling Fan Energy Efficiency,” Ernest Orlando Lawrence Berkeley National laboratory, 2012.
- [15] A. Jain, R. R. Upadhyay, S. Chandra, M. Saini and S. Kale, “Experimental Investigation of the Flow Field of a Ceiling Fan,” in *Proceedings of 2004 ASME Heat Transfer/Fluids Engineering Summer Conference*, North Carolina, USA, 2004.
- [16] Department of Energy, “Energy Conservation Program: Test Procedures for Ceiling Fans; Final Rule,” U.S. Department of Energy, 2017.
- [17] International Electrotechnical Commission, “IEC 60879:1986,” International Electrotechnical Commission, 1986.
- [18] American National Standards Institute, “Laboratory Methods of Testing Air Circulating Fans for Rating and Certification,” Air Movement and Control Association Inc., 2015.

- [19] Bureau of Energy Efficiency, “Schedule – 8 Ceiling Fans,” Bureau of Energy Efficiency, New Delhi, 2016.
- [20] The US Environmental Protection Agency, “Testing Facility Guidance Manual: Building a Testing Facility and Performing the Solid State Test Method for Energy Star Qualified Ceiling Fans,” Energy Star, Washington, 2002.
- [21] Department of Industry (Australia), “Review of Vietnamese Electric Fans Standards : A report for the Vietnam Energy Efficiency Standards and Labelling (VEESL) Program,” Kevin Lane, Mark Ellis, 2014.
- [22] J. Estevadeordal , S. Gogineni , W. Copenhaver , G. Bloch and M. Brendel , “Flow Field in a Low-Speed Axial Fan: a DPIV Investigation,” *Experimental Thermal and Fluid Science*, pp. 11-21, 2000.
- [23] Fluent Inc., “Fluent User's Guide,” ANSYS, Inc., 2009.
- [24] A. Jain, R. R. Upadhyay, S. Chandra, M. Saini and S. Kale, “Experimental Investigation of the Flow Field of a Ceiling Fan,” in *Proceedings of ASME Heat Transfer/Fluids Engineering Summer Conference*, North Carolina, USA, 2004.
- [25] P. Biermayer, J. Busch, S. Hakim, I. Turiel, P. d. Pont and C. Stone, “Feasibility of an Appliance Energy Testing and Labeling Program for Sri Lanka,” Ceylon Electricity Board, 2000.
- [26] US Energy Information Administration, “Use of Electricity,” US department of Energy, 30 4 2018. [Online]. Available: https://www.eia.gov/energyexplained/index.php?page=electricity_use. [Accessed 10 1 2018].
- [27] L. Huang, Q. Ouyang, Y. Zhu and L. Jiang, “A Study About the Demand for Air Movement in Warm Environment,” *Building and Environment*, no. 61, pp. 27-33, 2013.

- [28] Energy Star, "Ceiling Fans," Energy Star, 1 April 2012. [Online]. Available: https://www.energystar.gov/products/lighting_fans/ceiling_fans. [Accessed 5 May 2018].
- [29] M. Jain, A. B. Rao and A. Patwardhan, "Energy Efficiency Policies in India: Implications for Climate Change Mitigation," *Climate Change Signals and Response, A Strategic Knowledge Compendium for India*, no. 1, pp. 289-303, 2018.
- [30] Canadian Standards Association, "Energy Performance of Ceiling Fans," Canadian Standards Association, Ontario, 2015.
- [31] Bureau of Indian Standards, "Specification for Electric Ceiling Type Fans And Regulators," Bureau of Indian Standards, New Delhi, 2004.
- [32] A. G. T. Sugathapala , "Wall Effects on the Performance of Ceiling Fans: A Two-Dimensional Model," in *ERU Research Symposium, University of Moratuwa, Moratuwa, Sri Lanka*, 2000.
- [33] E. Adeeb, A. Maqsood and A. Mushtaq, "Effect of Number of Blades on Performance of Ceiling Fans," in *4th International Conference on Advances in Mechanics Engineering (ICAME 2015)* , 2015.
- [34] D.S. Parker and j. Sonne, "Measured Ceiling Fan Performance and Usage Patterns: Implications for Efficiency and Comfort Improvement," 1998.
- [35] Natural Resources Canada, "Ceiling fans (air flow) – March 2017, Technical bulletin on developing new standards," Office of Energy Efficiency, Canada, 03 2017. [Online]. Available: <https://www.nrcan.gc.ca/energy/regulations-codes-standards/19422>. [Accessed 21 12 2017].
- [36] S. R. Shah, S. V. Jain, R. N. Patel and V. J. Lakhera, "CFD for Centrifugal Pumps: A Review of the State-of-the-Art," in *Procedia Engineering*, Ahmedabad, 2013.

- [37] Resolved Analytics, “A Comparison of CFD Software Packages,” Resolved Analytics, 27 April 2017. [Online]. Available: <https://www.resolvedanalytics.com/theflux/comparing-popular-cfd-software-packages>. [Accessed 12 May 2018].
- [38] H. Versteeg and W. Malalasekera, *An introduction to Computational Fluid Dynamics, The Finite Volume Method*, London: Longman Scientific & Technical, 1995.
- [39] ANSYS Inc., “Fluent Theory Guide,” ANSYS Inc., 2009.
- [40] A. Pogorelov, M. Meinke and W. Schröder, “Large-Eddy Simulation of the Flow Field in a Rotating Axial Fan,” Springer International, Switzerland, 2016.
- [41] P. D. M. P. Rajapakshe, M. H. H. G. Mapa, R. Thanushan and R. A. C. P. Ranasinghe, “Investigating Aerodynamic Performance of a Ceiling Fan,” in *Annual Sessions of IESL*, Colombo, 2015.
- [42] A. Gerasimov, “Quick Guide to Setting Up LES-type Simulations,” Ansys, 2016.
- [43] Z. J. Zhai, W. Zhang, Z. Zhang and Q. Y. Chen, “Evaluation of Various Turbulence Models in Predicting Airflow and Turbulence in Enclosed Environments by CFD: Part 1 - Summary of Prevalent Turbulence Models,” *Hvac&R Research*, vol. 13, no. 6, pp. 853-870, 2007.
- [44] C. Qingyan, “Computational Fluid Dynamics for HVAC: Successes and Failures,” *ASHRAE Transactions*, vol. 1, no. 103, pp. 178-187, 1997.
- [45] P. Jones and G. Whittle, “Computational Fluid Dynamics for Building Air Flow Prediction—Current Status and Capabilities,” *Building and Environment*, vol. 4, no. 27, 1992.
- [46] Q. Chen, “Comparison of Different k- ϵ Models for Indoor Air Flow Computations,” *An International Journal of Computation and Methodology*, vol. 28, no. 3, pp. 353-369, 1995.
- [47] Z. Lin, T. T. Chow, Q. Wang, K. F. Fong and L. S. Chan, “Validation of CFD model for research into displacement ventilation,” *Architectural Science Review*, vol. 48, no. 4, pp. 305-316, 2005.

- [48] T. Kempe and A. Hantsch, "Large-Eddy Simulation of Indoor Air Flow Using an Efficient Finite-Volume Method," *Building and Environment journal*, vol. 115, pp. 291-305, 2017.
- [49] B. Joakim, A. Bergersen, K. Valen-Sendstad and M. Mortensen, "Implementation, verification and validation of large eddy simulation models in oasis," in *National conference on computational mechanics*, 2015.
- [50] J. Ma, F. Wang and X. Tang, "Comparison of Several Subgrid-Scale Models for Large-Eddy Simulation of Turbulent Flows in Water Turbine," in *The 4th International Symposium on Fluid Machinery and Fluid Engineering*, Beijing, 2008.
- [51] A. Giaque, J. Boudet, H. Ma and W. Wei, "Large Eddy Simulation of an Axial Compressor Rotor Passage : Preliminary Comparison with Experimental Measurements," in *22nd French Congress of Mechanics Proceedings*, Lyon, 2015.
- [52] A. Pogorelov, M. Meinke and W. Schröder, "Cut-Cell Method Based Large-Eddy Simulation of Tip-Leakage Flow," *AIP physics of Fluids*, no. 27, 2015.
- [53] S. Kang, "On the Onset of Wake Meandering for an Axial Flow Turbine in a Turbulent Open Channel Flow," *Journal of Fluid Mechanics*, vol. 744, no. May 2018, pp. 376-403, 2014.
- [54] T. Misaka, F. Holzäpfel and T. Gerz, "Large-Eddy Simulation of Aircraft Wake Evolution from Roll-Up Until Vortex Decay," *AIAA Journal*, vol. 53, no. 9, pp. 2646-2670, 2015.
- [55] T. Yamada and C. Kawakita, "Study on Practical CFD for Unsteady Vortices from Trailing Edge of Propeller Blades," *Mitsubishi Heavy Industries Technical Review*, vol. 52, no. 4, pp. 56-64, 2015.
- [56] V. Kolar, "Vortex Identification: New Requirements and Limitations," *International Journal of Heat and Fluid Flow*, no. 28, pp. 638-652, 2007.
- [57] F. D. Yves Dubief, "On Coherent-Vortex Identification in Turbulence," *Journal of Turbulence*, no. 1, 2000.

- [58] G. Wang, S. Moreau, F. Duchaine and J. d. Laborderie, “LES Investigation of Aerodynamics Performance in an Axial Compressor Stage,” no. June, 2014.
- [59] S. Bianchi, D. Borello, A. Corsini, F. Rsipoli and A. Sheard, “Large-Eddy Simulation of the Aerodynamic and Aeroacoustic Performance of a Ventilation Fan,” *Advances in Acoustics and Vibration*, vol. 2013, 20113.
- [60] Q. Liu, D. Qi and H. Tang, “Large Eddy Simulation of an Axial Compressor Rotor Passage : Preliminary Comparison with Experimental Measurements,” in *Proc. IMechE Vol. 221 Part C: J. Mechanical Engineering Science*, 2007.
- [61] Z. Lin, T. T. Chow, Q. Wang, K. F. Fong and L. S. Chan, “Validation of CFD Model for Research into Displacement Ventilation,” *Architectural Science Review*, vol. 48, no. 4, pp. 305-316, 2005.
- [62] J.F.vanderAuweraert, “Modeling of Wind Turbine Wake with a Sliding Mesh,” 2015.
- [63] D. Feldmann and C. Wagner, “Notes on Numerical Fluid Mechanics and Multidisciplinary Design,” *New Results in Numerical and Experimental Fluid Mechanics*, vol. VIII, pp. 591-598, 2013.
- [64] W. Chen, S. Liu, Y. Gao, H. Zhang, E. Arens, L. Zhao and J. Liu, “Experimental and Numerical Investigations of Indoor Air Movement Distribution with an Office Ceiling Fan,” *Building and Environment*, vol. 130, no. December 2017, pp. 14-26, 2018.
- [65] L. Prandtl, “Tragflügeltheorie,” *Königliche Gesellschaft der Wissenschaften zu Göttingen*, 1918.
- [66] Sri Lanka Standards Institution, “Sri Lanka Standard Energy Efficiency Rating for Electric Ceiling Fans With Regulators (Sri Lanka Standard 1600 : 2011),” Sri Lanka Standards Institution, Colombo, 2011.

- [67] The US Environmental Protection Agency, “ENERGY STAR Testing Facility Guidance Manual: Building a Testing Facility and Performing the Solid State Test Method for ENERGY STAR Qualified Ceiling Fans,” ENERGY STAR, Washington, 2002.
- [68] Sri Lanka Standards Institution, “Sri Lanka Standard 1600 : 2011 Energy Efficiency Rating for Electric Ceiling Fans With Regulators,” Sri Lanka Standards Institution, Colombo, 2011.
- [69] P. D. M. P. Rajapakshe, . M. H. H. G. Mapa, R. Thanushan and R. A. C. P. Ranasinghe, “Investigating Aerodynamic Performance of a Ceiling Fan,” in *Annual Sessions of IESL*, Colombo, 2015.
- [70] P. D. M. P. Rajapakshe, M. H. H. G. Mapa, R. Thanushan and R. A. C. P. Ranasinghe, “Investigating Aerodynamic Performance of a Ceiling Fan,” in *Annual Sessions of IESL*, Colombo, 2015.
- [71] Sri Lanka Standards Institution, “Sri Lanka Standard Energy Efficiency Rating for Electric Ceiling Fans with Regulators,” Sri Lanka Standards Institution, Colombo, 2011.